MEMORANDUM
RM-3566-PR
SEPTEMBER 1964

THE INVERSE PROBLEM OF THE LINEARIZED THEORY OF FULLY-CAVITATING HYDROFOILS

B. R. Parkin

PREPARED FOR:
UNITED STATES AIR FORCE PROJECT RAND

The RAND Corporation
SANTA MONICA • CALIFORNIA

MEMORANDUM
RM-3566-PR
SEPTEMBER 1964

THE INVERSE PROBLEM OF THE LINEARIZED THEORY OF FULLY-CAVITATING HYDROFOILS

B. R. Parkin

This research is sponsored by the United States Air Force under Project RAND—Contract No. AF 49(638)-700 monitored by the Directorate of Development Plans, Deputy Chief of Staff, Research and Development, Hq USAF. Views or conclusions contained in this Memorandum should not be interpreted as representing the official opinion or policy of the United States Air Force.

DDC AVAILABILITY NOTICE
Qualified requesters may obtain copies of this report from the Defense Documentation Center (DDC).

The RAND Corporation
1700 MAIN ST. • SANTA MONICA • CALIFORNIA • 90406

PREFACE

When pump blades or foils move with sufficiently high speeds in a liquid, it is found that the liquid cannot withstand the hydrodynamic tensions thus generated and boiling or cavitation occurs. Cavitating flows are two-phase flows consisting of a liquid and a gas which is composed of the liquid vapor and possibly some permanent gases. In an advanced stage, the cavitation consists of a long bubble in the wake of the blade or foil. The cavity thus formed originates from well-defined separation points on the body. When this situation is observed, the flow state is called a cavity flow or a fully-cavitating flow.

For some high-speed hydraulic machinery such as water, fuel or cryogenic liquid pumps, or in some marine propellers or on hydrofoil boats, the requirements of high speed causes cavitation to be inevitable. It then becomes necessary to deal effectively with such cavitating flows in order to obtain the best performance from a given machine. In particular, it is often necessary to operate in the fully-cavitating regime so that the hydrodynamics of fully-cavitating blades or foils become of fundamental importance.

In recent years it has become fashionable to predict these hydrodynamic properties by means of a linearized theory of cavity flows in order to secure the advantage of simplicity which linearization brings. As is also true of thin airfoil theory, linearization restricts the theories' range of applicability but it does permit one to attack some problems which might prove to be intractable if treated by more rigorous methods.

The present study originates from a review of linearized theory which was prepared by the author for the American Towing Tank Conference in 1959.* At that time it was found that although methods for the calculation of profile shapes from specifications of the pressure distribution on the wetted surface had been developed for a

---

*Parkin, B. R., Linearized Theory of Cavity Flow in Two Dimensions, The RAND Corporation, P-1745, July 15, 1959.

SUMMARY

This report presents the basic theory and some numerical results on the inverse problem for fully-cavitating hydrofoils. The problem is treated by the two-dimensional linearized theory of steady cavity flows. The problem of optimum hydrodynamic design of cavitating blades or foils is explored and the conditions required to insure realistic cavity flows are examined. As a result of these considerations three methods for profile design are put forward. Two of these methods are treated numerically. It is found that once the pressure distribution has been prescribed, the shape of the profile depends upon the design cavitation number. The camber decreases as the cavitation number increases. This report does not discuss the numerical methods used in the study. They are given separate documentation in RM-3563-PR, September 1964, by Mr. R. S. Grote.

limited range of application, there was still need for a more complete theoretical treatment of this important design technique. Since that time, further work by others has extended the range of these initial inverse theories. It is hoped that the present rather general treatment of the inverse problem for a single, isolated, fully-cavitating hydrofoil will add to the efforts of all who have worked to give the designer a better idea of performance goals which can be achieved with fully-cavitating lifting surfaces.

ACKNOWLEDGMENT

The author gratefully acknowledges the collaboration of Dr. T. W. Mullikin of RAND's Mathematics Department. His aid in the construction of the proof in Appendix C, which concerns the properties of the optimum pressure distribution, was a vital contribution to this study.

CONTENTS

PREFACE iii

SUMMARY v

ACKNOWLEDGMENT vii

Section
I. INTRODUCTION 1

II. SOME PRELIMINARIES 3

III. AN ELEMENTARY EXAMPLE 8

IV. GENERAL THEORY 18

V. THREE DESIGN METHODS 25

VI. LOW DRAG PROFILES 31

VII. CALCULATED RESULTS 38

VIII. CONCLUSIONS 46

Appendix
A. THE "OPTIMUM" PRESSURE DISTRIBUTION 47
B. PROFILE AND CAVITY CONTOURS AT THE DESIGN CONDITIONS 50
C. UPPER CAVITY CONTOUR FOR OFF-DESIGN CONDITIONS 52

REFERENCES 58

I. INTRODUCTION

Among the first problems studied in the early development of the two-dimensional linearized theory of cavity flows was the calculation of the wetted-surface shape of a profile from specifications upon its pressure (or vorticity) distribution.[1] In these previous studies other simplifications in addition to linearization of the problem have been introduced. For example in Ref. 1 the cavitation number is taken to be zero. Another simplification, adopted in Ref. 1 and in a considerable body of work which followed it,[2] is the restriction that the pressure distribution be specified in terms of truncated Fourier series. In all of these studies the design point is taken to be at the so-called "shockless entry" flow condition. For such flows, the upper surface of the cavity separates with a cusp from the leading edge of the profile and the theory predicts interference between the wetted surface of the foil and the upper surface of the cavity. Therefore, this design condition represents a fictitious flow state which cannot be achieved in practice. Recently Auslaender[3] has shown how this difficulty can be avoided and he has also considered the effect of free-surface proximity upon foil design at zero cavitation number. Still more recently, Oba[4] has given theoretical inverse calculations for a cavitation number of zero in an infinite fluid, which do not depend upon truncated Fourier series to represent the prescribed pressure distribution. He also assesses the accuracy of the linearized theory by comparing results from it with those obtained from exact, nonlinearized calculations.

In spite of the rather extensive developments indicated above, the general inverse problem for a single fully-cavitating hydrofoil at zero or nonzero cavitation number seems to have been neglected. The purposes of this paper are: (a) to show the effect of cavitation number upon profile design; (b) to reexamine the question of optimum profile design without the restrictions of shockless entry or of zero cavitation number; and (c) to sketch out numerical methods for the design of specific fully-cavitating hydrofoils. The methods of calculation, due to Mr. R. S. Grote, are elaborate. Because of this

complexity it does not seem feasible in this report to give them the careful consideration which they require. Therefore, Mr. Grote has given them separate documentation in Ref. 5. In the present calculations, the profile is taken to be deeply submerged so that, aside from those of the cavity itself, no free surface effects are considered. The methods used are those of linearized inverse airfoil theory, in which one specifies the pressure distribution on the profile and then calculates its shape.

II. SOME PRELIMINARIES

For completeness, our discussion starts with the complex perturbation velocity, $w(\zeta) = u - iv$, which defines the flow past a fully-cavitating cambered hydrofoil at a nonzero cavitation number. When the small perturbations are normalized with respect to q_c, the flow speed on the cavity surface, it is well-known that the complex velocity may be written in the form

$$w(\zeta) = \frac{2iA}{\zeta-1} + i\,\frac{B}{4}\,(\zeta - \frac{1}{\zeta}) + i(A+\alpha) - i\left[C_o + \sum_{n=1}^{\infty} C_n/\zeta^n\right] . \qquad (1)$$

In Eq. (1) α is the angle of attack, the C_n are real Fourier coefficients, and the coefficients A and B are real numbers. The complex variable ζ is derived from the complex variable $z = x + iy$ of the physical plane by the following mappings:

$$\nu = a\sqrt{\frac{z}{\ell - z}} \ , \quad \ell = a^2 + 1 \qquad (2)$$

and

$$\nu = \frac{1}{4}\,(\zeta + \frac{1}{\zeta}) - \frac{1}{2} \ . \qquad (3)$$

In the z-plane, the body consisting of the foil and its cavity is represented by a cut along the real z-axis from $x = 0$ to $x = \ell$, where $\ell > 1$. The wetted surface of the profile corresponds to that segment of the real axis in the interval

$$0 \leq xe^{2\pi i} \leq 1.$$

The upper surface of the cavity extends from the nose of the foil at $x = 0$ to the point at $x = \ell$. The lower surface of the cavity occupies the interval

$$1 \leq xe^{2\pi i} \leq \ell.$$

The transformation (2) maps the region outside the cut in the z-plane into the upper half of the ν-plane. The point $z = \infty$ is mapped into the point $\nu = ia$. The point $z = \ell$ is mapped into $\nu = \infty$. The upper surface of the cavity is mapped into the positive ν-axis. The wetted portion of the hydrofoil is mapped into the interval $-1 < \nu < 0$ with the profile nose at $\nu = 0$. The lower surface of the cavity extends along the remainder of the negative half of the real axis.
Equation (3) maps the wetted surface of the profile into the upper half of the unit circle in the ζ-plane with the nose at $\zeta = 1$ and with the trailing edge at $\zeta = -1$. The upper surface of the cavity occupies the positive real-axis outside $|\zeta| = 1$ and the lower surface of the cavity extends along all of the negative real axis outside the circle.

The function $w(z)$ satisfies the following conditions:

(i) $w(z) = -\beta$ at $z = \infty$,

where $\beta = 1 - \frac{1}{\sqrt{1+K}}$ and where K is the cavitation number defined as usual by

$$K = \frac{P_\infty - P_k}{\frac{1}{2}\rho U^2} .$$

Here U is the steady uniform velocity at $z = -\infty$, P_∞ is the static pressure at that point and P_k is the constant static pressure inside the cavity.

(ii) On the cavity surface $u = 0$.

(iii) The wetted surface of the profile is a streamline, that is:

$$\nu = -\alpha + \frac{d\eta}{dx} ,$$

where $\eta(x)$ is the camber function measured with respect to the profile chord.

This function determines the C_n in Eq. (1).

(iv) the cavity together with the foil constitutes a closed body. Thus,

$$\mathrm{Im} \oint w(z)\, dz = - 2\pi a_1 = 0,$$

where a_1 is the real part of the residue of $w(z)$ at $z = 0$.

(v) $w(z)$ is continuous at $z = 1$ (Kutta condition).

(vi) $u \leq 0$ everywhere in the flow.

In the problem considered below, the complex perturbation velocity must satisfy the six conditions noted above. However, we will first specify the perturbation pressure on the profile

$$p(x) = 2(P(x) - P_k) / \rho U^2 = - 2(1+K)\, u(x) \qquad (4)$$

and then employ condition (iii) in order to calculate the shape of the wetted surface, $\eta(x)$.

Equation (1) shows that if $A \neq 0$, $w(\zeta)$ is singular at the leading edge of the foil, $\zeta = 1$. Therefore the function p (or u) cannot generally be specified with complete arbitrariness on the wetted surface. On the other hand, it is possible to find an attack angle α for which the coefficient A vanishes. When this condition is satisfied the profile is said to be at the "ideal" attack angle corresponding to "smooth" or "shockless" entry. At this angle, one has greater control of the shape of the pressure distribution than is the case at other attack angles.* In general we shall imagine the pressure distribution on the foil to be the sum of two parts.

---

*At other angles the singular contribution from A, which has its own characteristic shape, may overshadow the effect of camber on the pressure distribution's shape. On the other hand, when we set $A = 0$ we remove one "degree of freedom" from the problem.

The first part, that due to the stagnation point at the leading edge, is associated with the nose singularity. We may adjust its magnitude but not its form. The second part, which is associated with the shape of the profile, may be thought to consist of the pressure distribution one prescribes at the ideal attack angle. The general shape of this part is subject to our pleasure but its amplitude may not always be specified arbitrarily. An important task of the present study consists of discerning the "poor" from the "advantageous" choices for the shape of this second part. Once a choice has been made, it may be necessary to adjust the amplitudes of the two parts so that an efficient profile, designed for a realistic cavity flow state, will result.

At points on the foil the function $i(\zeta - 1/\zeta)/2 = -\sin\theta$, so that the term involving the coefficient B in Eq. (1) contributes to u but not to v when $\zeta = e^{i\theta}$. On the other hand, Eq. (4) requires that the second part of $u(\theta)$ be specified as we may choose. For this reason we are led to add a term of the form $iB/2\zeta$ to $w(\zeta)$ in order to make this specification convenient. Therefore, for the present inverse problem we replace Eq. (1) by the particular solution.

$$w_p(\zeta) = iA + \frac{2iA}{\zeta-1} + i\frac{B}{4}\left(\zeta - \frac{1}{\zeta}\right) + i\frac{B}{2}\frac{1}{\zeta} + iD + w_1(\zeta). \qquad (5a)$$

The constant D of Eq. (5a) is given by

$$D = \alpha - C_o$$

and the term denoted by $w_1(\zeta)$ represents the contribution of the profile shape to the complex velocity. Thus the function w_1 is regular throughout the field of flow. Its real part must vanish on $\mathrm{Im}\zeta = 0$ and at $\zeta = \pm 1$ on the profile. Finally whenever the coefficient A is zero, at points on the foil, $u(\theta) = \overline{R\ell}\, w_1(e^{i\theta})$.

To complete the solution we can add to the particular solution of Eq. (5a) the complementary function $w_c(z)$. This function assumes the homogeneous boundary values,

$$u_c = 0, \quad 0 < x < \ell, \quad y = 0 \pm$$

and

$$v_c = 0, \quad \ell < x < 0, \quad y = 0.$$

At infinity, w_c is to be bounded. A function satisfying these conditions, which has no excess of sources or sinks, is

$$w_c(z) = -\frac{E}{2}\left[\sqrt{\frac{z}{z-\ell}} + \sqrt{\frac{z-\ell}{z}}\right], \tag{5b}$$

where the real constant E is taken to be positive or zero. Equation (5b) defines a flow having free streamlines above and below the real axis in the interval $0 \leq x \leq \ell$. If $y_c(1)$ denotes the ordinate of the upper free streamline at $x = 1$, as defined by the complementary function, then the constant E in Eq. (5b) is given by

$$E = y_c(1)/a.$$

Thus E can be defined in terms of the contribution made by the complementary function to the total cavity thickness at $x = 1$. Homogeneous solutions such as that of (5b) have been called "point drag force" solutions by Fabula.[6] Clearly, the complementary function has no effect upon the specification of the pressure p. Therefore the general solution for the inverse problem is given by the sum of Eqs. (5a) and (5b):

$$w(z) = w_P + w_c.$$

III. AN ELEMENTARY EXAMPLE

The general form of the complex velocity appropriate to the solution of the linearized inverse problem has been established by Eqs. (5a) and (5b). Moreover, we have indicated some of the important properties which the function w_1 must possess. We may add substance to this outline by means of a simple example of the inverse calculation method. To this end we transform the complex velocity of Eq. (5a) from the ζ-plane into the ν-plane, by means of Eq. (3), and obtain

$$w_p(\nu) = iA\sqrt{\frac{\nu+1}{\nu}} + iB\left(\frac{1+2\nu}{2}\right) + iD + w_1(\nu). \tag{6}$$

The function $w_1(\nu)$ may now be found from a knowledge of u on the real ν-axis. In principle this determination can always be carried out formally, provided that $u(\nu)$ is appropriately chosen in the interval $-1 \leq \nu \leq 0$. In the present example we will choose two points, ξ_o and ξ_1, such that $-1 \leq -\xi_1 \leq -\xi_o \leq 0$, and when $A = 0$ we shall require that $u(\xi)$ be specified by

$$u = \begin{cases} 0, & \nu \geq -\xi_o \\ -u_o, & -\xi_1 < \nu \leq -\xi_o, \\ 0, & \nu \leq -\xi_1 \end{cases} \tag{7}$$

where u_o is a positive constant. Let us consider the function

$$w_1(\nu) = i\frac{u_o}{\pi}\,\ell n\,\frac{\nu+\xi_o}{\nu+\xi_1}, \tag{8}$$

which is regular in the entire ν-plane exterior to the cut between the points $\nu = -\xi_o$ and $\nu = -\xi_1$. On the top edge of this cut, $R\ell w_1 = -u_o$ as required by Eq. (7). On the bottom edge of the cut, $R\ell w_1 = +u_o$ in conformance with the requirement that $w_1(\bar{\nu}) = -\overline{w_1(\nu)}$. Clearly, $R\ell w_1 = 0$ at points on the real axis outside the cut. Thus the function w_1 specifies the shape of the second part of the pressure distribution and the magnitude of A determines the amplitude of the first part.

Conditions (ii), (v), (vi) and Eq. (4) are now satisfied by Eqs. (6), (8) and, except for the specification of p(x), also by Eq. (5b). In order to satisfy conditions (i) and (iv), and to compute the profile shape in accordance with condition (iii), we will find the Laurent expansion of $w(z) = w_p + w_c$ about the origin in the z-plane. The required expansion is

$$w(z) = \left\{ A\frac{\sqrt{ia(1+ia)}}{a} + \frac{B}{2}(i-2a) + iD - E + i\frac{u_o}{\pi}\ell n\frac{\xi_o + ia}{\xi_1 + ia} \right\} - \left\{ A\frac{\sqrt{ia(1+ia)}}{4a(1+ia)} + \frac{aB}{2} + \frac{u_o}{2\pi}\left(\frac{a}{\xi_o + ia} - \frac{a}{\xi_1 + ia}\right) \right\}\frac{\ell}{z} - \left\{ A\frac{(3+2ia)\sqrt{ia(1+ia)}}{32a(1+ia)^2} + \frac{3aB}{8} + \frac{E}{8} + \frac{3au_o}{8\pi}\left(\frac{1}{\xi_o + ia} - \frac{1}{\xi_1 + ia}\right) + i\frac{a^2 u_o}{8\pi}\left(\frac{1}{(\xi_1+ia)^2} - \frac{1}{(\xi_o+ia)^2}\right) \right\}\frac{\ell^2}{z^2} + \cdots \quad . \tag{9}$$

Condition (i) leads to two equations:

$$\beta = -\frac{A\epsilon}{2\sqrt{a}} + aB + E + \frac{u_o}{\pi}\left(\tan^{-1}\frac{a}{\xi_o} - \tan^{-1}\frac{a}{\xi_1}\right) \tag{10}$$

and

$$0 = \frac{A}{2}\frac{\delta}{\sqrt{a}} + \frac{B}{2} + D + \frac{u_o}{2\pi}\ell n\frac{\xi_o^2 + a^2}{\xi_1^2 + a^2}, \tag{11}$$

where

$$\begin{Bmatrix} \delta \\ \epsilon \end{Bmatrix} = \left[\sqrt{a^2+1} + 1\right]^{1/2} \pm \left[\sqrt{a^2+1} - 1\right]^{1/2}.$$

The closure condition (iv) requires that

$$0 = \frac{A}{4}\frac{\epsilon + a\delta}{a\ell\sqrt{a}} + B + \frac{u_o}{\pi}\left(\frac{\xi_o}{\xi_o^2+a^2} - \frac{\xi_1}{\xi_1^2+a^2}\right). \tag{12}$$

These three equations involve the six parameters a, β, A, B, D and E. If any three of them are specified the flow is determined. When A = 0 it is seen that as $a \to \infty$ ($K \to 0$) the cavity closure singularity B tends to zero and that the coefficient D also vanishes. The vanishing of D will be recognized from the special theory at K = 0 which requires that $\alpha - C_o = 0$ in order to provide a finite pressure at the nose of the profile. As is also the case with the theory at K = 0, the difference $D = \alpha - C_o$ is the quantity determined by our extended theory. The separate values assumed by α and C_o as well as the magnitude of E are found by additional conditions which may be imposed upon the theory.

In order to illustrate this last point let us consider the special case of a profile operating at the ideal attack angle but with $E \neq 0$. Suppose the pressure is constant over the full chord length. In this case $\xi_o = 0$, $\xi_1 = 1$ and the imaginary part of w at points on the foil consists of

$$v_P(\xi) = -\frac{B}{2}(1-2\xi) - (\alpha - C_o) - \frac{u_o}{\pi} \ell n \left| \frac{\xi}{\xi - 1} \right| , \qquad (13a)$$

and

$$v_c(x) = -\frac{E}{2} \frac{\ell - 2x}{\sqrt{x(\ell - x)}} . \qquad (13b)$$

Then it follows from condition (iii) and Eq. (2) above that

$$\eta(x) = \left(C_o - \frac{B}{2}\right) x + aB \left[(1+a^2) \tan^{-1} \sqrt{\frac{x}{\ell - x}} - \sqrt{x(\ell - x)} \right] - E\sqrt{x(\ell - x)} +$$

$$+ \frac{u_o}{\pi} \left\{ \frac{1}{2} \ell n \left[1 + \frac{x}{\ell - x} \right] - a \tan^{-1} \sqrt{\frac{x}{\ell - x}} - x \ell n \, a\sqrt{\frac{x}{\ell - x}} - (1-x) \ell n \left[1 - a\sqrt{\frac{x}{\ell - x}} \right] \right\} . \qquad (14)$$

In the customary "direct theory" the forces on the foil become infinite as $a \to 0$. The very nature of the "inverse theory" developed here precludes this behavior of the forces. Instead the theory breaks down as $a \to 0$ by giving an indeterminate camber function. Equation (14)

furnishes an example of this behavior.

If E were zero, the coefficient C_o and the ideal attack angle α could now be found by the use of Eq. (11) and (12) (with A = 0) and by imposing the condition,

$$\eta(1) = 0 \ , \tag{15}$$

upon Eq. (14). Equation (15) is the requirement which must always be satisfied if the ordinates of the profile are to be measured from its chord line. However, $E \neq 0$ in general, so that Eq. (15) relates E and α. Thus from Eqs. (11), (12), (14) and (15) after some reduction we get

$$\alpha = \frac{u_o}{\pi} \frac{a^2}{1+a^2} + aE \ . \tag{16}$$

When E = 0 the angle α might be called the design angle of attack for smooth entry. Its variation with K may be found in terms of the parameter a with the help of

$$\beta = \frac{u_o}{\pi} \left[\frac{a}{1+a^2} + \tan^{-1} \frac{1}{a} \right] , \tag{10a}$$

which comes directly from Eq. (10) with E = 0. If $E \neq 0$ the values of α and E must be determined by a further condition on the problem. In this study we shall require that the vertical distance between the trailing edge of the wetted surface and the upper surface of the cavity at x = 1 have a value designated by T. Aside from the question of interference between foil and cavity, the smallest admissible value of T corresponds to that value which leads to E = 0. Negative values of E have no physical interest and we shall always take $E \geq 0$. The velocity components $v_p(\nu)$ and $v_c(x)$ at points on the upper surface of the cavity can be obtained from Eqs. (5a) and (5b) respectively. Integration of these velocities along the upper cavity from x = 0 to x = 1 leads to the required distance T. Thus we find an added relationship between α and E. Equation (16) can be used to eliminate α from this result so that we obtain

$$T = \frac{2u_o}{\pi}\frac{a^2}{\ell} + 2aE \ .$$

If we specify a value of T such that $E \geq 0$ we may use Eqs. (10) and (12) to eliminate E from this equation and thereby replace Eq. (10a) with

$$\beta = \frac{T}{2a} + \frac{u_o}{\pi} \tan^{-1}\frac{1}{a} \ . \qquad (10b)$$

If β, u_o and T are prescribed (10b) leads to the corresponding value of $\underline{a}$. The value of E then follows at once. If it should happen that $E < 0$ one puts $E = 0$ in the preceding equations and determines the value of $\underline{a}$ corresponding to the prescribed K value from Eq. (10a).

When the x-component of perturbation velocity along the foil is given by the constant value $u = -u_o$, the corresponding perturbation pressure is $p_o = C_L = 2(1+K)\ u_o$; so that the variation of α with K depends upon whether one chooses a fixed perturbation velocity or a fixed perturbation pressure for use in Eqs. (16) and (10). To show this difference when $A = E = \underline{0}$ we have evaluated these equations for two values of C_L and for two values of u_o. The numerical results are plotted in Fig. 1. The points marked with the symbols "A" and "B" in this illustration define two flow states at the ideal attack angle for which hydrofoil ordinates have been calculated in accordance with Eq. (14). The resulting shapes of the wetted surface have been plotted in Fig. 2 in order to show how the shape of the profile changes with K when the lift coefficient and shape of the pressure distribution are held constant.

Finally, if $\nu = -\xi$ is a point on the foil Eq. (6) shows $v(\xi)$ to have no explicit dependence upon the value of A. Therefore Eqs. (13) and (14) are valid for other than the smooth entry condition. It is only necessary to account for the effect which the value of A has upon the magnitude of B in these formulas. For example, let C_L' be the lift coefficient due to camber and let C_L be the total lift coefficient resulting from both the first and the second parts of the pressure distribution. Then for the present example we can use the result,

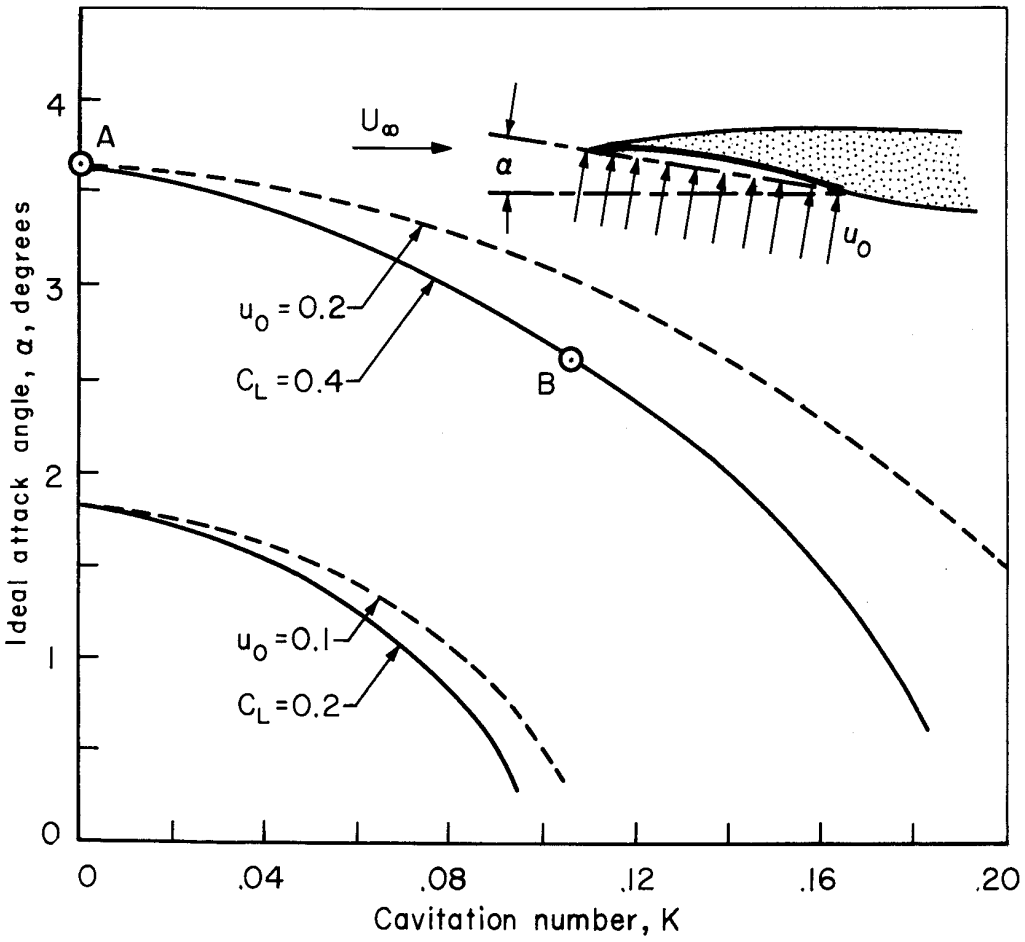

Fig. 1 — Design attack angles versus cavitation number for profiles having uniform pressure along the chord

$C_L = 4\pi(1+K)b_1$ where b_1 is the imaginary part of the residue from Eq. (9), to write

$$C_L = -\frac{A}{2}\pi(1+K)\left(\frac{\delta - a\epsilon}{\sqrt{a}}\right) + C_L' , \qquad (17)$$

where now

$$C_L' = 2(1+K)u_o .$$

If C_L and K values are specified and C_L' is chosen to be less than C_L,* then Eqs. (10), (11), (12) and (13) determine the values of A, B, a and D. Next, Eq. (15) together with the definition $D = \alpha - C_o$ yields the values α and C_o. Finally, the ordinates of the camber function for this profile at a nonideal attack angle follow from Eq. (14). The curve marked C in Fig. 2 shows the camber line for a profile having $C_L = .4$ but which has a uniform lift due to camber of $C_L' = .3$. The value of K is the same as that of point B in Fig. 1. In all cases it will be noted that the profile slope is vertical at the leading and trailing edges in accordance with the singular behavior of Eq. (13) at these two points. Because of this local breakdown of the linearized theory these profiles are of theoretical interest only. Finally, in Fig. 3 we compare with profile "B" of Fig. 2 a profile corresponding to the constant pressure and K values of point B of Fig. 1, but which as a positive E value such that T = 0.2. Although these two profiles have the same pressure distribution and value of K they certainly have different shapes. The drag of profile "E" exceeds that of profile "B".

In the preceding examples the value of the attack angle is determined in the course of the calculations. It should be emphasized that this is a rather special situation which comes about because of the fact that we have purposely considered cases in which either A or E, or perhaps both of them, are set equal to zero. More generally

*Throughout this work we take $C_L \geq C_L'$.

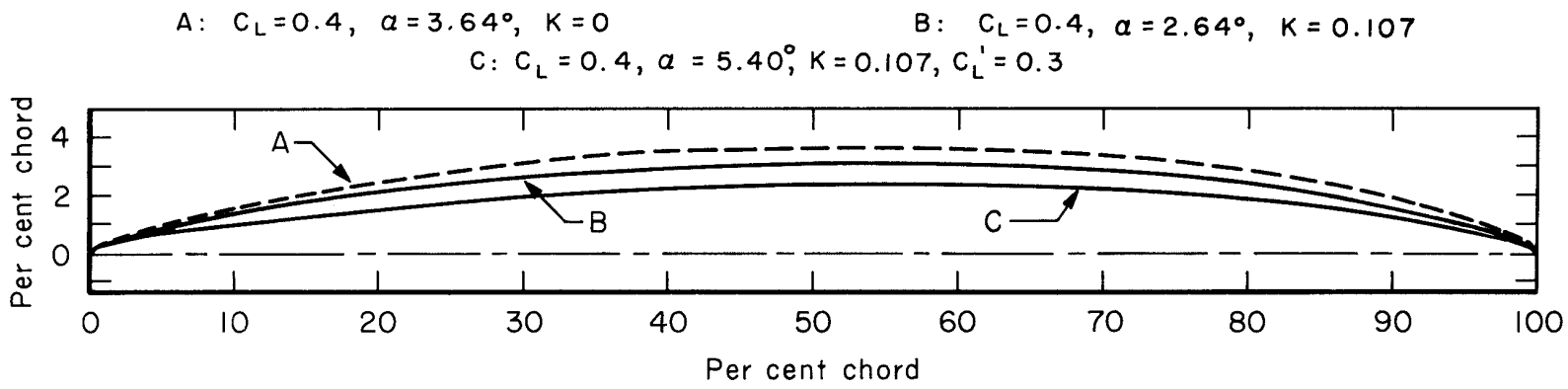

(A and B) Constant pressure across the chord at two cavitation numbers with smooth entry

(C) Three-fourths of C_L due to constant pressure distribution. Remaining part of C_L carried by nose distribution.

Fig. 2—Three profile shapes designed for $C_L = 0.4$

Vertical scale is twice horizontal scale in this illustration

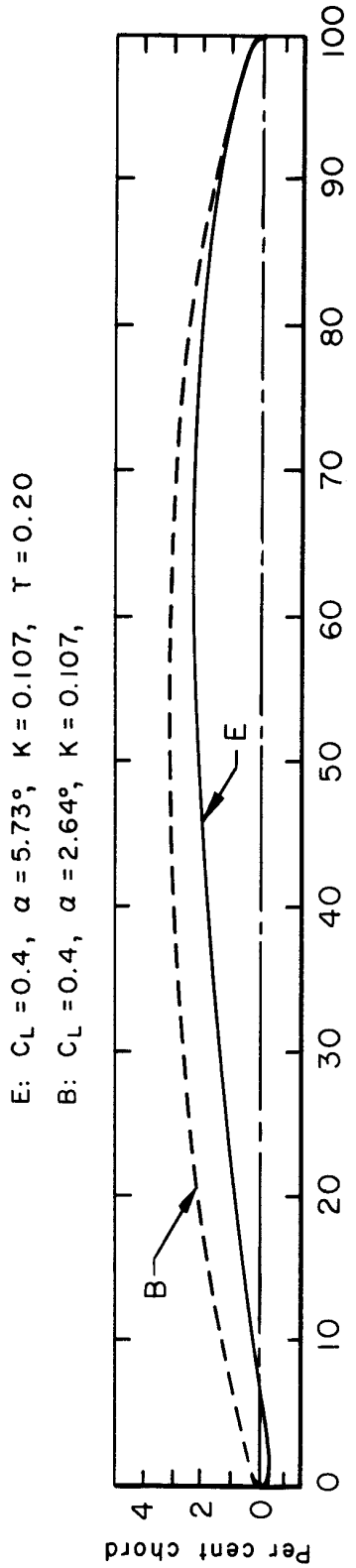

Fig. 3—Effect of complementary function on profile shape

Vertical scale is twice horizontal scale in this illustration

one may specify in advance the values of α, K, C_L and T, together with an appropriate shape for the second part of the pressure distribution and then determine the values of A and E which define the flow and the profile shape. This more general design problem is not considered in the present study. Instead we shall restrict our attention to the two limiting cases in which either A = 0 or E = 0.

IV. GENERAL THEORY

If we put $\xi_1 = 1$ in the various formulas of the preceding section, they become convenient building blocks for the construction of a general method of inverse hydrofoil calculations. For example, let us suppose for the moment that in the ν-plane that part of the perturbation pressure due to camber, $p(\xi)$, is given on the foil where $0 < \xi \leq 1$, $(\nu = -\xi)$. Then if we replace u_o in the preceding formulas by the differential

$$du_o = \frac{p'(\xi_o)d\xi_o}{2(1+K)} \quad ,$$

we may integrate Eq. (8) over the foil in order to obtain the net effect of the prescribed pressure distribution upon the complex velocity of Eq. (6). In order to satisfy conditions (i) and (iv) we can interchange the order of summation and integration for those terms in the Laurent expansion (9) which involve the term u_o. Then, conditions (i) and (iv) will lead to formulas for the determination of the constants B, K, etc., which contain integrals instead of the purely algebraic formulas given previously. In fact, these steps indicate that we need only integrate the terms containing u_o in Eqs. (10), (11) and (12) in order to obtain the results of interest here.*

If we carry out this integration after setting $\xi_1 = 1$ in Eq. (12) we find for B that

$$B = -\frac{A}{4}\frac{\epsilon+a\delta}{a\ell\sqrt{a}} + \frac{1}{2\pi(1+K)}\int_o^1 \left(\frac{1}{1+a^2} - \frac{\xi_o}{\xi_o^2 + a^2}\right) p'(\xi_o)d\xi_o \quad .$$

---

*Actually, integral superposition is applied only to w_1 in order to obtain a more general expression for this function than that of Eq. (8). Subsequent use of the expansion of Eq. (9) and the integrations indicated, allow us to proceed directly to the solution of the problem without explicitly calculating this more general form of w_1. Integral superposition cannot be applied to the problem as a whole because the cavity length of the fundamental solution, Eq. (8), depends upon ξ_o. It is obvious that Poisson's formula can also be applied to the solution of the present problem.

An integration by parts gives

$$B = -\frac{A}{4}\frac{\varepsilon+a\delta}{a\ell\sqrt{a}} + \frac{1}{2\pi(1+K)}\int_0^1 \frac{a^2-\xi^2}{(a^2+\xi^2)^2}\, p\,(\xi)\,d\xi, \tag{18}$$

provided that $p(0) = 0$. Similarly Eq. (11) can be transformed into

$$D = (\alpha - C_o) = -\frac{A}{2}\frac{\delta}{\sqrt{a}} - \frac{B}{2} + \frac{1}{2\pi(1+K)}\int_0^1 \frac{\xi p(\xi)\,d\xi}{\xi^2+a^2}\,. \tag{19}$$

In these more general circumstances Eq. (17) has the form

$$C_L - C_L' = \left\{C_L - \int_0^1 p(x)\,dx\right\} = -\frac{A}{2}\,\pi(1+K)\,\frac{\delta-a\varepsilon}{\sqrt{a}}\,, \tag{17a}$$

and if we integrate Eq. (10) and use Eqs. (2), (17a) and (18), it follows that

$$(1+K)\beta = \frac{C_L-C_L'}{2\pi\,\ell}\,\frac{(2a^2+3)\varepsilon+a\delta}{\delta-a\varepsilon} + (1+K)E + \frac{1}{2\pi\ell}\int_0^1 \sqrt{\frac{\ell-x}{x}}\,p(x)\,dx. \tag{20}$$

As will be discussed more fully below, if the coefficient E is arbitrarily set equal to zero and K, C_L, C_L' and $p(x)$ are prescribed in advance, the value of ℓ may be determined by Eq. (20). In the more general cases when C_L' is not known or when E is not necessarily zero, the value of ℓ must be found from the solution by means of an additional condition upon the position of the upper surface of the cavity.* Possible forms of this condition will be noted later. For the present it is sufficient to observe that values of the coefficients A, B, D and E can be found so that general expressions for the camber function and the upper contour of the cavity can be evaluated in particular cases. General formulas for the calculation of these two contours can be obtained as follows.

---

*As noted above, this study treats only solutions for which $E \geq 0$.

In order to compute the camber function $\eta(x)$ we need the imaginary part of the function $w_1(\nu) = u_1 - iv_1$ of Eq. (6) at points on the real axis in the ν-plane. We may obtain the required result by integrating the imaginary part of Eq. (8) over the foil as just discussed in connection with the derivation of Eqs. (18), (19) and (20). Alternatively we observe that on the real axis u_1 is known everywhere since it is equal to $-p(\xi)/2(1+K)$ on the foil and it must vanish on the cavity. Thus we may proceed directly to the desired result by use of the Hilbert transform,

$$v_1(\xi) = -\frac{1}{\pi} P \int_0^1 \frac{u_1(t)dt}{t-\xi} ,$$

where as usual $\nu = -\xi$ denotes a point on the foil.

Now we can replace Eq. (13) by

$$v_p(\xi) = -\frac{B}{2}(1-2\xi) - (\alpha-C_o) + \frac{1}{2\pi(1+K)} P \int_0^1 \frac{p(t)dt}{t-\xi} , \tag{21a}$$

and

$$v_c(x) = -\frac{E}{2} \frac{\ell-2x}{\sqrt{x(\ell-x)}} . \tag{21b}$$

In Eq. (21a) the quantities B and $(\alpha-C_o)$ are determined by Eqs. (18) and (19). Next we can apply condition (iii) to obtain for the camber function

$$\eta(x) = (C_o - \frac{B}{2})x + aB\left[\ell \tan^{-1}\sqrt{\frac{x}{\ell-x}} - \sqrt{x(\ell-x)}\right] - E\sqrt{x(\ell-x)}$$

$$+ 2a^2\ell \int_0^{\xi(x)} \frac{\xi v_1(\xi)d\xi}{(a^2+\xi^2)^2} , \tag{22}$$

where $\xi(x)$ is calculated from Eq. (2) and where $v_1(\xi)$ denotes the last term of Eq. (21a).

The upper contour of the cavity $y(x)$ may be found from the same sort of calculations as those leading to the camber function. On the upper surface of the cavity, $\nu \geq 0$ and the vertical component of the

perturbation velocity is composed of

$$v_P(\nu) = - A\sqrt{\frac{\nu+1}{\nu}} - (\frac{B}{2} + D) - B\nu + v_2(\nu)$$

and

$$v_c(x) = \frac{E}{2} \frac{\ell-2x}{\sqrt{x(\ell-x)}} ,$$

where

$$v_2(\nu) = \frac{1}{2\pi(1+K)} \int_o^1 \frac{p(\xi)\, d\xi}{\xi + \nu} .$$

It follows that the upper surface of the cavity has ordinates determined by

$$y(x) = -2a^2\ell A\, F_1(\nu,a) - (\frac{B}{2} + D)x + aB\left[\sqrt{x(\ell-x)} - \ell \tan^{-1}\sqrt{\frac{x}{\ell-x}}\right] +$$

$$E\sqrt{x(\ell-x)} + 2a^2\ell \int_o^{\nu(x)} \frac{\nu v_2(\nu)d\nu}{(a^2+\nu^2)^2} . \qquad (23)$$

The function $F_1(\nu,a)$ is defined in Appendix C below. It is possible to invert the order of integration in the integrals of Eqs. (22) and (23). The results of this step are given in Appendix B.

Once a satisfactory solution has been obtained the remaining hydrodynamic characteristics of the profile can be calculated. For example the moment coefficient referred to the hydrofoil nose is

$$C_M = - \left\{C_L - \int_o^1 p(x)dx\right\} \frac{(3+a^2)\delta - 2a(2+a^2)\epsilon}{8\epsilon\sqrt{\ell}} - \int_o^1 x\, p(x)dx . \qquad (24)$$

Nose-up moments are taken to be positive. The first term in Eq. (24) gives the contribution of the coefficient A [see Eq. (17a)] to C_M. This term may be derived with the aid of the result that $C_M = -4\pi(1+K)b_2$, where b_2 is the imaginary part of the coefficient of $1/z^2$ in (9). Of course, only that term in Eq. (9) which involves A explicitly

contributes to the first term of (24). The last term gives the contribution of the lift due to camber. Whether or not E = 0, Eq. (24) gives the correct value of C_M because the symmetry of the complementary function does not permit it to contribute to the moment. Finally the drag coefficient may be calculated whether A = 0 or not by making use of the expansion of w(z) about the end of the cavity, namely:

$$w(z) = - (aB + \frac{E}{2}) \sqrt{\frac{\ell}{z-\ell}} + O\ (|z-\ell|^{1/2}).$$

For then, the drag coefficient is proportional to the square of the coefficient of $(z-\ell)^{-1/2}$. Thus,

$$C_D = 2\pi(1+K)\ \ell(aB + \frac{E}{2})^2$$

and it follows that

$$C_D = \frac{1+a^2}{2\pi(1+K)} \left\{ \frac{C_L-C_L'}{\ell} \frac{\epsilon+a\delta}{\delta-a\epsilon} + a \int_0^1 \frac{a^2-\xi^2}{(\xi^2+a^2)^2}\, p(\xi)d\xi + \pi(1+K)E \right\}^2. \tag{25}$$

In the limit as K → 0 these formulas become

$$C_M = - \frac{5}{16} \left\{ C_L - C_L' \right\} - \int_0^1 x\, p(x)dx \tag{24a}$$

and

$$C_D = \frac{1}{2\pi} \left\{ 2(C_L-C_L') + \int_0^1 p(\xi)d\xi + \pi\, y_c(1) \right\}^2. \tag{25a}$$

In (25) and (25a) $\xi = \xi(x)$ is obtained from Eq. (2) by putting $\nu = - \xi$ and $z = xe^{2\pi i}$. It is worth noting that Eqs. (25) and (25a) show that the cavity drag can originate from three sources. These sources are: the nose singularity or angle of attack term, the prescribed pressure due to camber, and the homogeneous or complementary function. Moreover, since C_L-C_L', p(x) and E are all greater than or equal to zero, it follows, except for certain pathological cases

which we shall exclude, that each of these terms adds to the total cavity drag. None of them acts to reduce the value of C_D.

The formulas of this section permit the determination of the shape of fully-cavitated hydrofoil profiles under rather broad conditions. However, there is a theoretical restriction on the form of the function $p(x)$ which must be disposed of before we can turn to practical questions of profile design. The point in question concerns the behavior required of $p(x)$ at the profile trailing edge. Actually this requirement is contained implicitly in the seven conditions on $w(z)$ which have been listed previously. However, the importance of this condition in the present problem merits an explicit development.

In order to consider the behavior of $w(z)$ in the neighborhood of $z = 1$, we put $t = z-1$ and consider the nature of $w(t)$ near $t = 0$. On the lower surface of the cavity $t > 0$ and $u = 0$. On the wetted surface of the foil $t < 0$ and $v = S_-(x)$, say. Moreover, on the real axis as $t \to 0_+$, $u \to 0$; and as $t \to 0_-$, $v \to S_-(0)$. Since $u = 0$ along $t > 0$ it follows from the principle of reflection that $w(\bar{t}) = -\bar{w}(t)$ so that v is even and u is odd in Im t. Hence it follows that

$$w(t) \sim i\sqrt{t}\sum_{0}^{\infty} a_n t^n - iS_-(0) + O(1)$$

where the a_n are real and the order term is imaginary. From condition (vi) we must have $u \leq 0$ for $-\pi \leq \arg t \leq 0$, so that $a_0 \leq 0$ and $a_n = 0$ for $n = 1, 2, \ldots$. Hence in the z-plane we may write

$$w(z) \sim ia_0\sqrt{z-1} - i\,S_-(1) + O(1)\ ;$$

so that at points on the foil for which $z = xe^{2\pi i}$, we have

$$u = -\frac{p}{2(1+K)} \sim a_0\sqrt{1-x}.$$

We shall take the positive square root. The fact that $a_0 \leq 0$ suggests that we put $a_0 = -\lambda$ where $\lambda \geq 0$. Then we can express $p(x)$ as

$$p(x) \sim 2(1+K)\ \lambda\ \sqrt{1-x} \qquad (26)$$

near $x = 1$. The property of the function $p(x)$ indicated by Eq. (26) requires some attention in the numerical calculations.

V. THREE DESIGN METHODS

The general formulas of the preceding section permit us to consider specific profile designs. However, the elementary example studied previously indicates that one may wish to carry out these inverse calculations using various design philosophies. For this reason, the present section treats three calculation schemes which, in principle at least, include all possibilities.

The first method, which concerns profile design at the ideal attack angle, is the one calculation in which the designer has the greatest degree of control over the whole pressure distribution and over the design cavitation number. Because of this fact, he might be justified in regarding this case as the proper linearized inverse hydrofoil problem.

As we have already seen, the ideal angle exists when $w(z)$ has no stagnation-point singularity at the leading edge. For this case $A = 0$ in all formulas of the preceding section. In order to determine a realistic flow we require that the upper surface of the cavity must not interfere with the wetted surface of the profile. One way to insure that this requirement will be met is to introduce a "trailing edge thickness" T which, for this problem, will be defined as the vertical distance between the upper surface of the cavity and the trailing edge of the wetted surface. After a value of T has been chosen, the solution may show that the cavity intersects the wetted surface forward of the trailing edge or that the clearance between the wetted surface and the upper surface of the cavity is too small. Then it would be necessary to repeat the calculation with a larger value of T. This troublesome occurrence is not as likely in practical applications of the first method as it is in the other methods given below.

Since we specify T in advance, there is now an added condition,

$$\alpha + y(1) = T, \tag{27}$$

which completes the determination of the flow. In fact if one puts $A = 0$ and $x = 1$ in Eq. (23) and then uses Eqs. (15) and (20) to eliminate α and E from Eq. (27), he finds after some manipulation that a can be determined from

$$\beta = \frac{T}{2a} + \frac{1}{4\pi(1+K)a}\int_0^1 p(x)\ell n\left|\frac{a\sqrt{x}+\sqrt{\ell-x}}{a\sqrt{x}-\sqrt{\ell-x}}\right| dx\ . \quad (28)$$

If one were willing to design for a predetermined value of a rather than for a specified value of K, Eq. (28) could be solved with little trouble. However, since one almost always needs to design for some particular value of K, Eq. (28) must be solved for a by iteration. The mapping (2) is determined once a has been found so that B and then D may be calculated from Eqs. (18) and (19). As a result of the steps leading to the derivation of Eq. (28) it follows that one can now calculate E from the formula

$$E = \frac{T}{2a} - B\left(a-\ell\tan^{-1}\frac{1}{a}\right) - \frac{1}{2\pi(1+K)}\left\{\left(a+\ell\tan^{-1}\frac{1}{a}\right)\int_0^1 \frac{p(\xi)d\xi}{\xi^2+a^2}\right.$$
$$\left. - 2\ell\tan^{-1}\frac{1}{a}\int_0^1 \frac{\xi^2 p(\xi)d\xi}{(\xi^2+a^2)^2} - a\ell\int_0^1 \frac{\xi p(\xi)d\xi}{(\xi^2+a^2)^2}\ell n\left|\frac{\xi+1}{\xi-1}\right|\right\}, \quad (29)$$

where the integrations are carried out in the ν-plane. It is unlikely that Eq. (29) will ever lead to negative values of E. However, if this should happen, one could then put $E = 0$ and calculate with the formulas of the preceding section in which both $A = 0$ and $E = 0$.

---

*If one sets p(x) constant, transforms the variable of integration to the ν-plane, and integrates by parts, he can recover Eq. (10b). Similarly one can integrate Eq. (29) and note that for p(x) constant, $B = p_o/2\pi(1+K)\ell$. After some manipulation he finds that T is given by the equation just preceding (10b). Equation (30) integrates directly to give $C_o = \frac{T}{2} + \frac{B}{2} - \frac{p_o}{4\pi(1+K)}\ell n\frac{\ell}{2a}$, which can also be obtained from the constant pressure results given previously.

The value of C_o is given by

$$C_o = \frac{T}{2} + \frac{B}{2} + \frac{1}{2\pi(1+k)} \left\{ -\int_o^1 \frac{\xi p(\xi)\,d\xi}{a^2+\xi^2} - a^2 \ell \ell n\left(1+\frac{1}{a^2}\right)\int_o^1 \frac{\xi p(\xi)\,d\xi}{(a^2+\xi^2)^2} \right.$$

$$\left. + a^2 \ell \int_o^1 \frac{\xi p(\xi)\,d\xi}{(a^2+\xi^2)^2} \ell n \left| \left(1-\frac{1}{\xi}\right)\left(1+\frac{1}{\xi}\right) \right| \right\}, \qquad (30)$$

and the design attack angle follows from

$$\alpha = C_o + D.$$

The profile ordinates and slope may then be calculated from Eqs. (21) and (22), the moment coefficient can be found from Eq. (24) and the drag coefficient determined from Eq. (25).

In the limit as $K \to 0$, Eq. (28) indicates that $a \to \infty$, and in accordance with the discussion which follows Eq. (5b) we require that

$$aE \to y_c(1).$$

Then we have:

$$\alpha = \frac{T}{2} + \frac{1}{2\pi}\int_o^1 \xi p(\xi) \ell n \left| \left(1-\frac{1}{\xi}\right)\left(1+\frac{1}{\xi}\right) \right| d\xi ,$$

$$y_c(1) = \frac{T}{2} - \frac{1}{\pi}\left\{ \int_o^1 p(\xi)\,d\xi - \frac{1}{2}\int_o^1 \xi p(\xi) \ell n \left| \left(1+\frac{1}{\xi}\right)/\left(1-\frac{1}{\xi}\right) \right| d\xi \right\},$$

$$\eta(x) = \alpha x - y_c(1)\sqrt{x} - \frac{1}{\pi}\left\{ \sqrt{x}\int_o^1 p(\xi)\,d\xi + \int_o^1 \xi p(\xi) \ell n \left| 1-\frac{\sqrt{x}}{\xi} \right| d\xi \right\},$$

$$\eta'(x) = \alpha - y_c(1)/2\sqrt{x} + \frac{1}{2\pi} P \int_o^1 \frac{p(\xi)\,d\xi}{\xi - \sqrt{x}},$$

$$y_{\blacksquare}(x) = \alpha x + y_c(1)\sqrt{x} + \frac{1}{\pi}\left\{ \sqrt{x}\int_o^1 p(\xi)\,d\xi - \int_o^1 \xi p(\xi) \ell n \left(1+\frac{\sqrt{x}}{\xi}\right) d\xi \right\},$$

and from Eq. (25a)

$$C_D = \frac{1}{2\pi}\left\{\int_0^1 p(\xi)d\xi + \pi y_c(1)\right\}^2 .$$

The preceding integrations are carried out in the ν-plane and the ordinates of the upper surface of the cavity, $\bar{y}$, are measured from the hydrofoil chord line.

The second method accounts for the fact that, at a prescribed value of C_L, interference between the hydrofoil and the cavity can be eliminated by increasing the attack angle of the profile instead of by means of the complementary function. In this case $E = 0$ and $A \leq 0$ in the formulas of the preceding section. Although we can prescribe the value of C_L in advance, we cannot prescribe all features of the pressure distribution. Only the shape of that part of the pressure distribution which is associated with camber is subject to our pleasure. Thus, as discussed previously, we consider the total pressure distribution to be composed of two parts: one part which is due to the nose singularity and the other part which is due to the shape of the wetted surface. The shape of the first part is fixed, but we can vary its amplitude by varying the magnitude of A. Once the shape of the second part has been prescribed we shall adjust its amplitude so that the value of C_L, due to both the first and the second parts, stays constant. Thus, when $A = 0$ we see from Eq. (17a) that $C_L = C_L' = \int_0^1 p(x)dx$, where the function $p(x)$ determines the shape of the pressure distribution due to camber. In order that we can adjust this part, let us put

$$C_L' = m\int_0^1 p(x)dx = m\, C_L ,$$

where $o \leq m \leq 1$. Replacing C_L' in (17a) by this expression, we write Eq. (17a) as

$$(1-m)C_L = -\frac{A}{2}\pi(1+K)\frac{\bar{\delta}-a\epsilon}{\sqrt{a}} . \qquad (17b)$$

Evidently when m = 1, A = 0.

For the second design method we can put E = 0 and insert the above value of C_L' in Eq. (20). Then we can eliminate m and α from this new form of Eq. (20), (15), and (27) in order to obtain a relationship which defines a. This equation is

$$\left[(1+K)\beta - \frac{(2a^2+3)\epsilon+a\delta}{2\pi\ell(\delta-a\epsilon)} C_L\right]\left\{\frac{a}{\ell}\int_0^1 \sqrt{\frac{\ell-x}{x}}\, p(x)dx - \int_0^1 p(x)\ell n \frac{\sqrt{\ell-x}+a\sqrt{x}}{\sqrt{\ell}}\, dx\right.$$

$$\left. + \frac{1}{2}\int_0^1 p(x)\ell n(1-x)dx - \left(4a^2\ell\sqrt{a}\, F_1(1,a) + \frac{\epsilon+a\delta}{\ell}\left[a-\ell\tan^{-1}\frac{1}{a}\right]\right)\frac{C_L}{\delta-a\epsilon}\right\} =$$

$$\frac{1}{2\pi\ell}\left[\pi(1+K)T - \left(4a^2\ell\sqrt{a}\, F_1(1,a) + \frac{\epsilon+a\delta}{\ell}\left[a-\ell\tan^{-1}\frac{1}{a}\right]\right)\frac{C_L}{\delta-a\epsilon}\right]\cdot$$

$$\left\{\int_0^1 \sqrt{\frac{\ell-x}{x}}\, p(x)dx - \frac{(2a^2+3)\epsilon+a\delta}{\delta-a\epsilon} C_L\right\}. \qquad (31)$$

As in the case of Eq. (28), Eq. (31) must also be solved for a by iteration. Once a has been found the value of m follows from Eq. (20):

$$m = \left[2\pi\ell(1+K)\beta - \frac{(2a^2+3)\epsilon+a\delta}{(\delta-a\epsilon)} C_L\right] \Big/ \left[\int_0^1 \sqrt{\frac{\ell-x}{x}}\, p(x)dx - \frac{(2a^2+3)\epsilon+a\delta}{\delta-a\epsilon} C_L\right]. \qquad (32)$$

The attack angle is now determined by

$$\alpha = \frac{A}{4\sqrt{a}}\left[(\epsilon+a\delta)\tan^{-1}\frac{1}{a} - \frac{a\epsilon+(3a^2+2)\delta}{\ell}\right] + \frac{m}{2\pi(1+K)}\left\{\frac{a}{\ell}\int_0^1 \sqrt{\frac{\ell-x}{x}}\, p(x)dx\right.$$

$$\left. + \int_0^1 p(x)\ell n(1-x)dx - \int_0^1 p(x)\ell n \frac{a\sqrt{x}+\sqrt{\ell-x}}{\sqrt{\ell}}\, dx - \frac{1}{2}\int_0^1 p(x)\ell n\, x\, dx\right\}. \qquad (33)$$

The value of A is calculated from Eq. (17b) and all the remaining calculations can be completed with the general formulas of Section IV. In all of these formulas* the integrals involving p(x) or $p(\xi)$ must now be multiplied by m and the quantity E must be set equal to zero where ever it appears.

*Equation (31) and (32) are excepted.

Again, when K = 0, $\underline{a} = \infty$ and B = 0. Moreover, for the second method $y_c(1) = 0$. Therefore, the only unknowns are m and α. They are determined from Eqs. (15) and (27) with the understanding that the limiting expression for A is

$$A = -\frac{2}{\pi}(C_L - C_L') \ .$$

Then we find that

$$m = \left(\pi T - C_L\left[3\sqrt{2} - \ell n(1+\sqrt{2})\right]\right)\left\{2\int_0^1 p(\xi)\,d\xi + \int_0^1 \xi p(\xi)\,\ell n\,\frac{1-\xi}{1+\xi}\,d\xi - \left[3\sqrt{2} - \ell n(1+\sqrt{2})\right]C_L\right\}^{-1}$$

and that

$$\alpha = \frac{2(1-m)}{\pi}C_L + \frac{m}{\pi}\left\{\int_0^1 p(\xi)\,d\xi + \int_0^1 \xi p(\xi)\ \ell n\left|1-\frac{1}{\xi}\right|\,d\xi\right\} \ ,$$

where the integrations are carried out in the ν-plane.

The third method of profile design is more general than the two methods outlined above. In this method, instead of choosing either A = 0 or E = 0 at the start, we specify the value of α along with the values of C_L, K and p(x). We may then calculate the values of A, E and $\underline{a}$ from the theory. The general formulas of the preceding section, together with appropriate results given for the first two methods of this section, contain all ingredients required for this calculation. However, because we have made no numerical calculations in accordance with it in the course of this study, the details of this method are not considered here. The first two methods are limiting cases of the third method. However, in order that the conditions $A \leq 0$ and $E \geq 0$ will be satisfied in this case, the prescribed value of α must lie between the values determined by Eqs. (30) and (33). Therefore, the third method requires that the first and second problems are at least partly solved as a preliminary condition to its use.

VI. LOW DRAG PROFILES

The preceding results permit the design of fully-cavitating hydrofoil sections having predetermined specifications on their pressure distributions. As yet, however, we have made no attempt to discern "good" pressure distributions from "bad" ones. Such a determination rests mainly with the form of the function $p(x)$ which determines the profile camber. For the purposes of this study, a good choice for the function $p(x)$ would lead to a profile shape, having prescribed values of C_L and K, which for a given design method would have as low a value of C_D as possible and still satisfy all conditions required to guarantee a realistic cavity flow.

As noted previously, the form of Eqs. (25) or (25a) indicates that nonzero values of A (negative) and E (positive) always tend to increase, never to decrease, that value of C_D which would be obtained if the amplitude of $p(x)$ were fixed and A and E were made to vanish. Thus, once $p(x)$ is fixed, foils designed in accordance with the first method will always have higher drag than would result if it were possible to design with $E = 0$. The situation with regard to the second method is not as clear as it is for the first method, because in the second case the amplitude of $p(x)$, but not its shape, is allowed to vary in order to hold C_L constant regardless of the magnitude of A. On the other hand, it seems likely for either design method that if the shape of $p(x)$ is varied, the magnitudes of E or of A required to give realistic flows will change even though C_L, K and other parameters are fixed in advance. Therefore, the total effect on C_D of changes in the shape of $p(x)$ are not entirely predictable. Nevertheless, when $A = E = 0$ it would seem advantageous to determine the general form of $p(x)$ which leads to as low a cavity drag as possible for prescribed values of C_L and K. For, even though realistic solutions are not obtained in this limiting situation, it would seem that a good choice for the shape of $p(x)$ at the ideal attack angle when $A = E = 0$ will be almost as advantageous a choice for more realistic profile design. This conjecture can be tested by numerical calculation once the desirable properties for $p(x)$ have been determined.

When $A = E = 0$ it follows that $C_L = C_L'$, $C_M = C_M'$ and $C_D = C_D'$. Moreover, Eq. (25) then shows that when $K > 0$ the integrand of the expression between curly brackets will change sign if $\underline{a} < 1$. Therefore, if $p(\xi)$ is chosen appropriately there may be some conditions for which the drag will vanish. For example, if we put a Dirac δ-function of the form

$$p(\xi) = \frac{(\xi_o^2 + a^2)^2}{2a^2 \ell \xi_o} C_L' \, \delta(\xi - \xi_o), \quad 0 \leq \xi_o \leq 1, \tag{34}$$

in Eq. (25) we obtain

$$C_D' = \frac{1}{2\pi(1+K)a^2\ell} \left[\frac{a^2 - \xi_o^2}{2\xi_o} C_L' \right]^2, \tag{35}$$

which vanishes whenever $\underline{a} = \xi_o$. Clearly if $K > 0$, C_D vanishes whenever the strength of the closure singularity, B, vanishes. Some consequences of this fact will be noted below.

Now we observe that when $A = E = 0$, we can write the identities

$$C_L' = \int_o^1 p(x)dx \equiv 2a^2(1+a^2) \int_o^1 \frac{\xi p(\xi)}{(a^2+\xi^2)^2} d\xi \tag{36}$$

for the lift coefficient and from Eq. (24),

$$C_M' = -\int_o^1 xp(x)dx \equiv -2a^2(1+a^2)^2 \int_o^1 \left(\frac{\xi}{a^2+\xi^2}\right)^3 p(\xi)d\xi, \tag{37}$$

for the moment coefficient. If we take the limit as $\underline{a} \to \infty$ in these equations and also in Eq. (25), the transformed integrals on the right hand side of these equations become the well-known "equivalent airfoil" formulas of Tulin and Burkart.[1] In this special case for which $K = 0$, it is known that the pressure distribution which gives the lowest value of C_D' for any specific value of C_L' consists

of the δ-function at the trailing edge of the foil. This result may be seen directly from the "equivalent airfoil" integrals. Because of this special result for flows at K = 0 it seems natural to set $\xi_o = 1$ in Eqs. (34) and (35) and then to compare the drag from Eq. (35) with that resulting from any other pressure distribution when respective values of C_L' and of K are taken to be equal for both pressure functions.

Thus one may use the properties of the integrals of Eqs. (36), (37) and (25) to prove formally the following theorem: At the ideal attack angle all foils, having non-negative pressure distributions which are the sum of a Lebesgue integrable function and a countable number of Dirac δ-functions with finite total, will have a greater value of C_D' for prescribed values of C_L' and K, than will another profile at the same K and C_L' but which has a positive pressure distribution consisting of a δ-function at its trailing edge. The value of a for this δ-function profile must exceed unity. The proof of this result is given in Appendix A.

Whenever it holds, the above theorem seems to contain more generality than is required to show that at the ideal angle all profiles having pressure distributions of practical interest will have greater drag than the "optimum" δ-function profile. When A and E = 0, if we write Eq. (20) as an integral in the ν-plane we have

$$(1+K)\beta = \frac{a^3}{\pi}\int_0^1 \frac{p(\xi)\,d\xi}{(a^2+\xi^2)^2}, \tag{20a}$$

and if we make use of Eqs. (34) and (35), we may characterize this "optimum" performance by

$$\left(\frac{L}{D}\right) = \frac{8\pi(1+K)}{C_L'}\,\frac{a^2(a^2+1)}{(a^2-1)^2}, \tag{38}$$

where

$$a = \frac{C_L'}{4\pi(1+K)\beta} + \sqrt{\left(\frac{C_L'}{4\pi(1+K)\beta}\right)^2 - 1}\,. \tag{39}$$

At K = 0 Eqs. (38) and (39) reduce to the Tulin-Burkart value, $(L/D) = 8\pi/C_L$, $a = \infty$.

Although the preceding results have been developed from formulas designed to satisfy the six fundamental conditions listed previously, we already know that because both A and E are zero, the "optimum" δ-function pressure distribution does not lead to physically meaningful flows.

Moreover just the fact that, for a δ-function pressure, a flow state can exist for which the cavity drag vanishes, that is to say $B = 0$, warrants further investigation of the flows corresponding to δ-function profiles. In connection with the vanishing of the coefficient B we observe that ordinarily this quantity is a positive number. When $B > 0$ it can be seen from Eq. (6) by letting $\nu \to \infty$ along the bottom and top surfaces of the cavity, that at the end of the cavity, v, the y-component of velocity, approaches $-\infty$ on the upper surface and $+\infty$ on the lower surface. Thus, the end of the cavity is smoothly rounded as one expects the present linearized theory to predict. When $B = 0$ the velocity is bounded at $x = \ell$ and the resulting cavity is closed by a cusp and $C_D' = 0$. When $B < 0$ the y-component of velocity tends to $+\infty$ on the upper surface and to $-\infty$ on the lower surface as the end of the cavity is approached. This reversal of the flow direction as B changes sign suggests that the cavity has suffered a radical change of shape.

The degree to which the δ-function pressure distribution fails to give a physically meaningful flow is indicated by Fig. 4 which shows some profile and cavity contours for various cavitation numbers when the point-force is at the trailing edge of the foil. Although the profile shows some very slight changes in shape with changing K, these differences cannot be disclosed by a drawing to the scale of Fig. 4. Therefore, all profile shapes are represented by the single, heavier curve. The changes in cavity shape with changing K are quite pronounced. The most striking feature revealed by Fig. 4 is that even for low K values the cavity-body system is not a simple closed curve. The δ-function pressure obviously leads to a fictitious flow. On the other hand as long as $\underline{a} \geq 1$ the cavity contours (on a two-sheeted

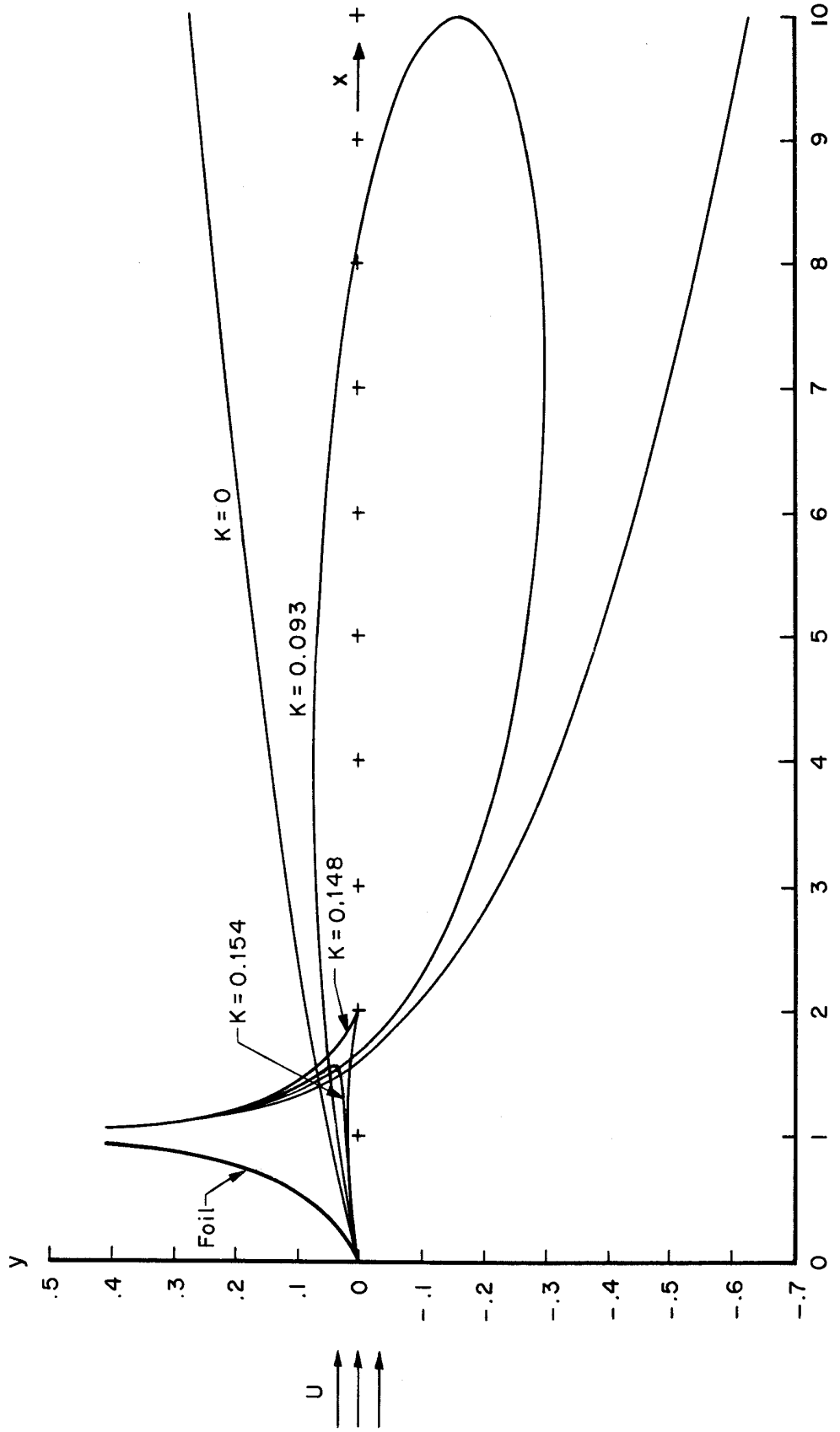

Fig. 4 — Calculated foil and cavity shapes for the delta function loading, $p(\xi) = (\ell^2/2a^2)\, C_L \delta(\xi - 1)$, at four cavitation numbers with $C_L = 1.0$

Vertical scale 5 times horizontal scale

surface) are convex with respect to the flow region as required by condition (vi).* When $\underline{a} < 1$, the cavity is completely turned inside out and at some points its curvature changes sign so that condition (vi) is violated for this case. In all cases condition (v) is violated, although if one were to change the inequality at the end of Eq. (34) to read $0 \leq \xi_o < 1$ this situation would no longer be strictly true. Nevertheless, the small perturbation assumption would certainly be violated in the neighborhood of the trailing edge. The remainder of the six fundamental conditions are satisfied formally at least, although to say that the cavity-body system represents a "closed" body simply means that there are no excess sources or sinks inside it. The double valuedness of the present flows must cause us to reject all such point-force solutions as linearized cavity flows.

Although the δ-function profile is certainly not an optimum section under any physically meaningful circumstance, the flow associated with this pressure distribution has been found to satisfy formally several of the six fundamental conditions. Moreover, one can regard a δ-function pressure distribution as being a limiting form of an ordinary continuous distribution in which the continuous distribution of pressure is replaced by a point force at its center of pressure. Therefore, for profiles having continuous pressure distributions with a specified C_L' at the ideal angle, we might interpret the preceding theorem as indicating that the nearer the center of pressure is to the trailing edge of the foil, the lower will be the value of C_D'. This interpretation has been tested numerically for two values of C_L'. The numerical results are summarized in Table 1. For simplicity, the calculations are based upon the parabolic pressure functions $p(x) = 6\, C_L' (1-x)x$ for $0 \leq x \leq 1$ and $p(x) = 15\, C_L'[(9-5x)x-4]$ for $.8 \leq x \leq 1$, $p(x) = 0$ for $0 \leq x \leq .8$. In the first case the center of pressure is located at the half-chord point, and in the second case the center of pressure is located at $\bar{x} = .9$. It may be noted that

---

*If the radius of curvature at any point along a stream filament in an irrotational flow is R and if the direction of the positive normal, n, points toward the center of curvature, the normal component of the pressure gradient is $dp/dn = -\rho q^2/R$, where q is the velocity along the stream filament.

these functions are of such form

Table 1

NUMERICAL VALUES FOR SHOCKLESS ENTRY

$\bar{x}$	K	C_L'	C_M'	C_D'	a	α
.5	.03	.4	-.20	.0153	6.632	2.283^o
.9	.03	.4	-.36	.0048	4.095	-7.47^o
.5	.0096	.1	-.05	.000957	5.154	$.572^o$
.9	.0096	.1	-.09	.000279	3.092	-1.915^o

that $\lambda = 0$ in Eq. (26). The trends shown in Table 1 support the correctness of the interpretation indicated above. All previous results known from the special theory at $K = 0$ have also shown this trend of decreasing C_D' as the center of pressure is moved towards the trailing edge of the profile.

VII. CALCULATED RESULTS

The preceding sections have illustrated qualitative aspects of the inverse theory, have given formulas and procedures for profile design and have indicated the kind of pressure distributions which may be advantageously prescribed. It remains now to give more concrete evidence of the efficiency of these methods. Again, we note that the numerical methods which lead to the results discussed here are not considered in this report. These important matters are given a full exposition in Ref. 5.

The numerical examples treated in this memorandum are based upon a modified form of Johnson's "three-term" pressure distribution.[2] The modification consists of the removal of a small lump in pressure between $x = 0$ and $x = 1/16$. The distribution of pressure is given parametrically by

$$x = [(1 - \cos \theta)/2]^2$$

and

$$p(x) = \begin{cases} 0 \ , & 0 \leq \theta \leq \frac{\pi}{3} \ , \\ \frac{C_L}{1.1365} \left[\sin \theta - \sin 2\theta + \frac{1}{2} \sin 3\theta\right] \ , & \frac{\pi}{3} \leq \theta \leq \pi \ . \end{cases}$$

The shape of this pressure distribution is shown in Fig. 5 for a C_L of .4. The rearward location of the center of pressure may be noted.

With this pressure distribution as a basis, calculations have been carried out in accordance with the first and second design methods for a trailing edge thickness, $T = 0.2$. In order to emphasize the effect of cavitation number upon the shapes of the wetted surface and the upper surface of the cavity, calculations are presented for $K = 0$ and $K = 0.2$. Figure 6 shows plots of the cavity contours (upper part) and camber lines (lower part) resulting from calculations

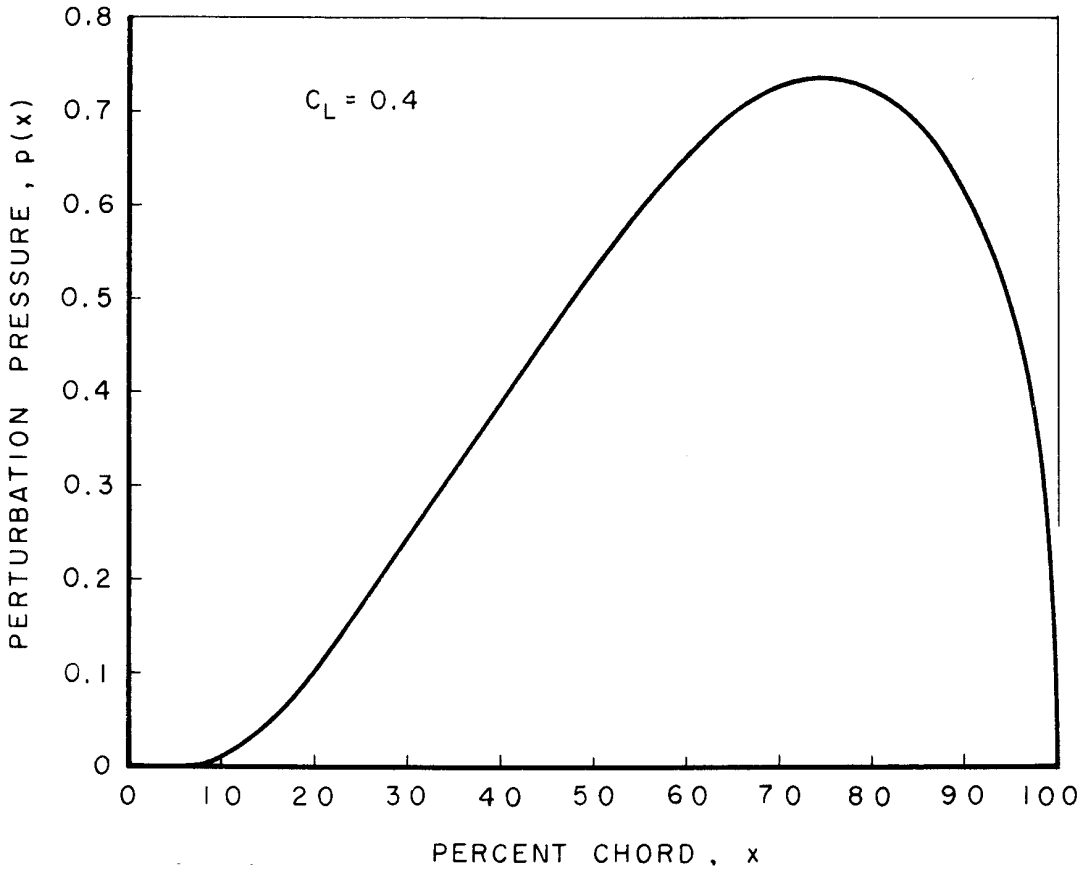

Fig. 5 — A modified three term pressure distribution

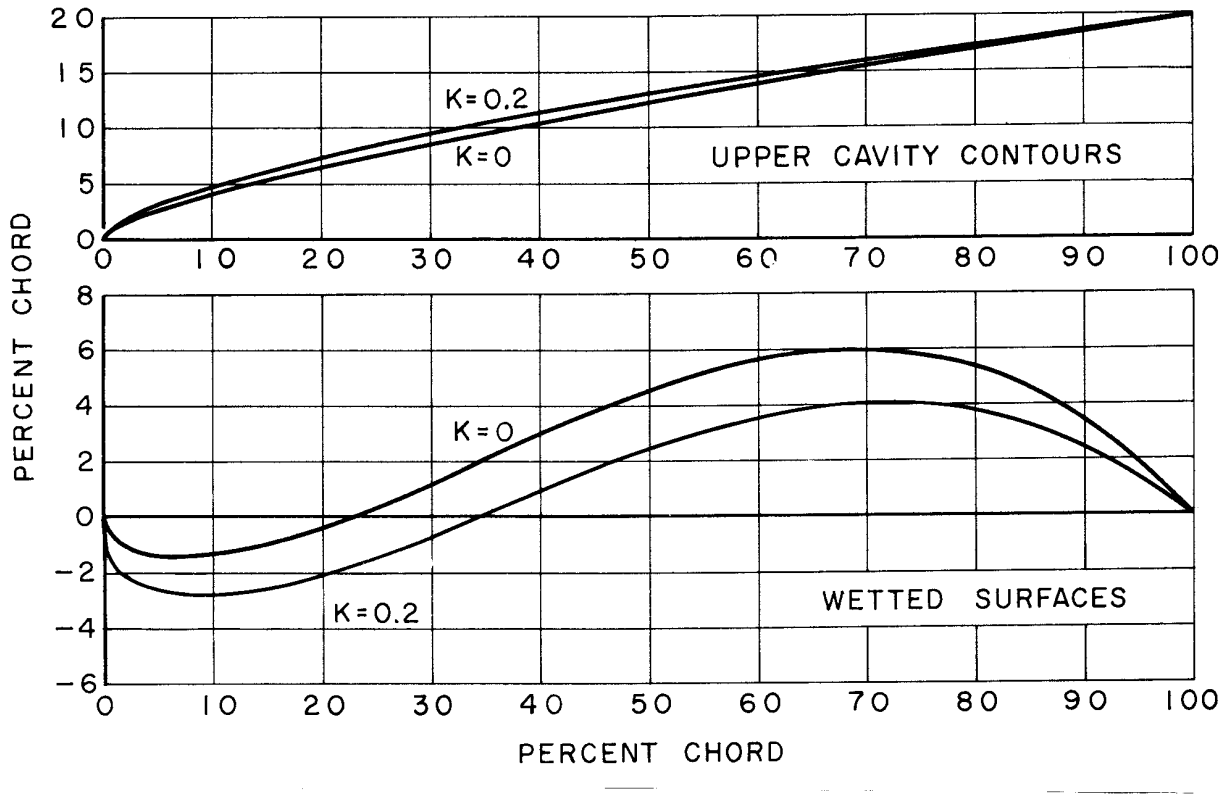

Fig. 6 — Cavity contours and wetted-surface shapes for two cavitation numbers calculated from the pressure distribution of Fig. 5 in accordance with the first design method.

Vertical scale is magnified in the lower graph

in accordance with the first method. The abscissa of all curves in Fig. 6 is the profile chord line. The scale of ordinates in the lower plot has been chosen to give vertical distances a 2.5 magnification with respect to the horizontal in order to facilitate comparison. Figure 7 illustrates to the same scale as Fig. 6, the contours obtained when the calculations are carried out in accordance with the second method of profile design. The trend of decreasing camber with increasing cavitation number, discussed previously in Section III, is shown again in these illustrations. A new ingredient is the change in the shape of the upper cavity as the cavitation number increases. It may seem surprising at first that, except at the trailing edge, the cavity contour at the larger cavitation number is farther above the chord line than it is at K = 0. As will be seen shortly, this state of affairs is caused by the fact that the attack angle at the larger cavitation number is greater than it is at K = 0. The considerable difference in profile shape resulting from the two design methods is also clearly shown by these two illustrations.

Table 2 below summarizes the hydrodynamic parameters calculated for these four profiles. Comparison

Table 2

HYDRODYNAMIC PROPERTIES OF FOUR PROFILES

K	C_L	C_D	$L/_D$	C_M	α	ℓ	E	m	A	design method
0	.4	.0509	7.85	-.267	4.27^o	∞	--	1.	0	#1
0	.4	.0411	9.74	-.221	5.98^o	∞	0	.548	-.115	#2
.2	.4	.0561	7.13	-.267	4.51^o	4.42	.0555	1.	0	#1
.2	.4	.0447	8.94	-.166	6.71^o	3.53	0	.290	-.133	#2

of the L/D values from this table tends to show that at any K-value it is more efficient hydrodynamics to cause the cavity to clear the profile by increasing the attack angle than it is to use the "point-drag" singularity for this purpose. In some practical situations this gain in hydrodynamic design may not be available if structural requirements strongly favor the thicker nose offered by the first design method. In any case, these data argue for the desirability

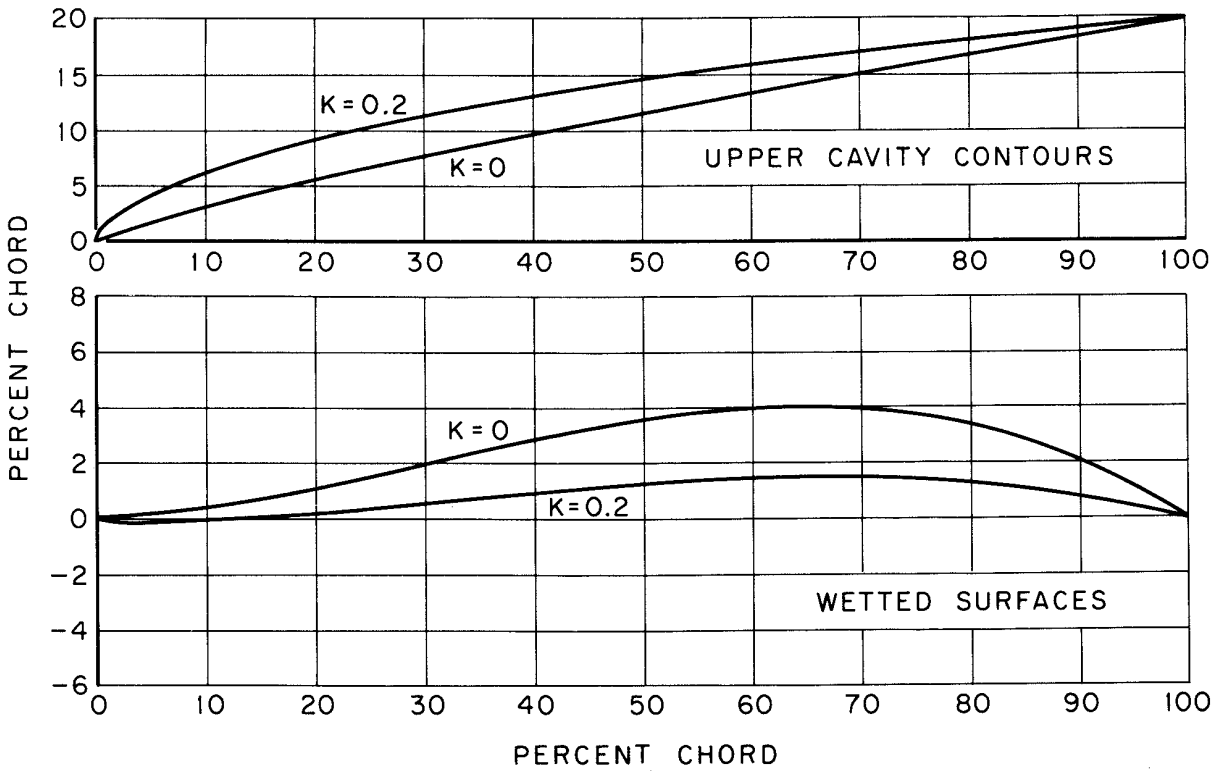

Fig. 7 — Cavity contours and wetted-surface shapes for two cavitation numbers calculated from the pressure distribution of Fig. 5 in accordance with the second design method.

Vertical scale is magnified in the lower graph

of implementing the third design method in order that both structural and hydrodynamic design requirements can be matched as fully as possible. At K = 0 the present data show that the L/D of the second foil design exceeds that of the first design by 24% while at K = .2 the superiority of the second profile design is 25%. These figures also seem to show that the L/D attainable with the first method decreases somewhat more rapidly with increasing values of cavitation number than do L/D values obtained from the second method. The decreases in the two cases are 9.2% and 8.2%, respectively. The forward movement of the center of pressure which accompanies the increase of α in the case of the second design method is shown by the C_M values in Table 2.

Johnson has indicated[2] that the three-term section should have L/D = 35.3. His value corresponds to a flow state for which, in our terminology, both E and A are zero. In this case the cavity interferes with the wetted surface of the foil. The present results illustrate the drag increase one must accept in order to obtain a profile designed for realistic operating conditions.

Finally, the off-design forces can be calculated by using the function $d\eta/dx$ obtained from the inverse calculations in a solution of the direct problem such as that of Ref. 7. Such additional calculations of the hydrodynamic coefficients for the above profiles are not considered here. However, some off-design calculations of the sort discussed in Appendix C, which determine those values of α, K and $\underline{a}$ which cause the cavity to become tangent to the upper surface of the foil, have been carried out. In these calculations the upper surface of the profile is assumed to have ordinates equal to 90% of the cavity ordinates at the design point, thereby defining a profile which is just inside the cavity at the design condition. An example from calculations by the second method for such a foil is illustrated in Fig. 8. As before, the calculations were carried out for a design condition of T = .2 and C_L = .4. The design cavitation number in this example is .01. The single point plotted in Fig. 8 shows the design α of 6^o. The effect of reducing the profile thickness to 90% of the upper cavity ordinates puts the design point inside the region

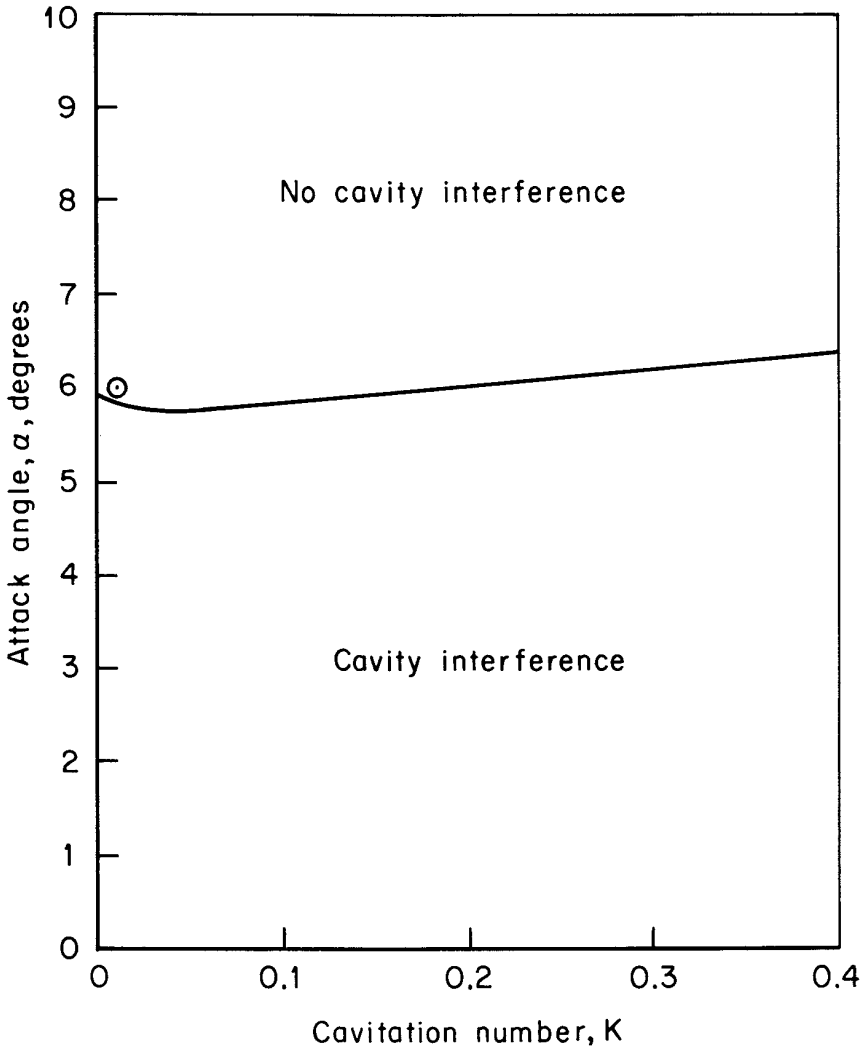

Fig. 8 — Possible flow regimes for a three term profile

of no cavity interference. The curve shows the locus of points for which the upper cavity is just tangent to the upper surface of the profile at a point between its nose and tail. In this example the point of tangency is at the trailing edge except for K-values at and very close to zero. This forward movement of the tangent point is accompanied by the rise in α, as $K \rightarrow 0$, shown in the figure. This figure shows quite clearly that the selection of parameters C_L and T in the present study can lead to rather high-attack angle requirements with the result that the predictions of the linearized theory lose accuracy. Fortunately, this effect on L/D is not as pronounced.[7] The choice of smaller values of C_L and T would have led to profiles for which the effects of linearization are not as important. The present example has been chosen simply to illustrate the effectiveness of the present theory rather than to put forward specific profile designs.

VIII. CONCLUSIONS

The aim of this study has been to investigate the general inverse problem for fully-cavitating hydrofoils within the framework of the linearized theory of cavity flows and to explore the problem of optimum hydrodynamic design without regard for structural considerations. We have found that, in a strict sense, there is no definite solution to the optimization problem but that if one imposes added conditions upon the class of solutions admitted it sometimes becomes possible to pick an "optimum" from among that particular class. More generally, we have found that at any prescribed values of K and C_L the cavity drag becomes less as the center of pressure is moved nearer to the trailing edge, provided the profile operates at the smooth (or shockless) entry condition. Those conditions which must be added to this requirement on the shape of the pressure distribution in order to insure a practically attainable cavity flow have been studied with the result that three design procedures have been proposed. Two of these have been implemented numerically.[5] Once the pressure distribution has been prescribed it has been found that the shape of the profile depends upon the design cavitation number. The general trend is that the camber decreases as K increases. The importance of this factor for practical design may be noted. Another finding is that there are two distinct ways of making sure that the cavity will clear the foil. One way depends on the use of the homogeneous solution for the symmetrical cavity flow problem and the other depends upon designing at attack angles greater than those for shockless entry. Of these two, the latter method appears to give more efficient designs from a purely hydrodynamic point of view. However, structural requirements often override purely hydrodynamic considerations with the result that it would seem best if one were to design using a third method which employs both ways of avoiding interference between the foil and the cavity.

Appendix A

THE "OPTIMUM" PRESSURE DISTRIBUTION*

Subject to the restriction that the δ-function profile is to operate at the ideal angle (A = E = 0) in a flow for which the cavity length parameter of the δ-function profile satisfies the condition $\underline{a} > 1$, we shall demonstrate the following proposition: Let two flows contain fully-cavitating profiles which satisfy Eqs. (17) through (25) of the text. Suppose these two cavity flows have the same value of the cavitation number K and that the two foils operate at the same value of C_L. Let the pressure distribution of one of the foils be characterized by any nonnegative function $p(\xi)$ which consists of a Lebesgue integrable part plus possibly a countable and summable number of Dirac δ-functions. Then if the pressure distribution of the second profile consists of a δ-function at its trailing edge, it follows that this profile will experience a lower value of C_D than will the first foil which has the pressure function $p(\xi)$ as defined above.

Let us reserve the designation δ-function profile for foils with a δ-function pressure distribution at the trailing edge, $\xi = 1$. Let the lift and drag coefficients of this foil be denoted by C_{L_δ} and C_{D_δ}. From Eqs. (34), (35) and (20a) we have

$$C_{D_\delta} = \frac{1}{2\pi(1+K)a^2\ell}\left[\frac{a^2-1}{2} C_{L_\delta}\right]^2 \tag{A1}$$

and

$$(1+K)\beta = \frac{a}{2\pi\ell} C_{L_\delta} . \tag{A2}$$

---

*This proof was constructed with the collaboration of Dr. T. W. Mullikin of the Mathematics Department, The RAND Corporation.

In order to carry out the proof we proceed in two steps. Firstly, we shall show that the δ-function profile has the lowest drag when a and K are held fixed. Secondly, we will show that the δ-function profile will still have the lowest drag if K is held fixed as before but a and C_{L_δ} are allowed to vary so that the C_L of the δ-function profile may be made equal to that of the nonoptimum profile.

The first part of the proof is started by forming the ratio of Eq. (20) to (36). Thus when A = E = 0,

$$(1+K)\beta/C_L = \frac{1}{2\pi}\frac{a}{\ell}\int_0^1 \frac{p(\xi)d\xi}{(a^2+\xi^2)^2} \Bigg/ \int_0^1 \frac{\xi p(\xi)}{(a^2+\xi^2)^2}\, d\xi.$$

Equation (A2) may be put in this result, so that

$$C_{L_\delta}\int_0^1 \xi \frac{p(\xi)}{(a^2+\xi^2)^2}\, d\xi = C_L \int_0^1 \frac{p(\xi)}{(a^2+\xi^2)^2}\, d\xi. \tag{A3}$$

Since $\xi \leq 1$ and $a > 1$, we have $a^2 - \xi^2 \geq a^2 - 1 > 0$ and we may transform Eq. (25) into the inequality,

$$C_D > \frac{a^2\ell}{2\pi(1+K)}\left\{(a^2-1)\int_0^1 \frac{p(\xi)}{(a^2+\xi^2)^2}\, d\xi\right\}^2 .$$

Now we may use (A3) and Eq. (36) to write this inequality as

$$C_D > \frac{1}{2\pi(1+K)a^2\ell}\left[\frac{a^2-1}{2} C_{L_\delta}\right]^2 . \tag{A4}$$

By virtue of (A1) we may write (A4) as

$$C_D > C_{D_\delta} , \tag{A5}$$

and the first part of the proof is complete.

The second part of the proof depends upon the fact that

$$C_{L_\delta} > C_L \ . \tag{A6}$$

This inequality follows at once from Eq. (A3) and the fact that $0 \leq \xi \leq 1$. Now we may consider a third profile in a flow satisfying conditions (i) through (vi) and having the same value of K as the flows above. Imagine this third foil to have a pressure distribution which also consists of a δ-function at $\xi_o = 1$, but which may have any values of $\underline{a}'$ and C_L' satisfying Eq. (39). Denote its drag coefficient by C_D'. As before, we require that $\underline{a}' \geq 1$. Then it follows from Eq. (39) that $\underline{a}' \leq \underline{a}$ if we put $C_L' = C_L$, and from Eq. (35) it follows at once that $C_D' \leq C_{D_\delta}$ so that (A5) is still satisfied.

Appendix B

PROFILE AND CAVITY CONTOURS AT THE DESIGN CONDITIONS

If as suggested in the text, the order of integration is inverted in Eq. (22) and the integrations are carried out, the profile shape is:

$$\eta(x) = (C_o - \frac{B}{2})\, x + aB\left[\ell \tan^{-1}\sqrt{\frac{x}{\ell-x}} - \sqrt{x(\ell-x)}\right] - E\sqrt{x(\ell-x)}$$

$$+ \frac{1}{2\pi(1+K)}\left\{x\int_o^1 \frac{\xi p(\xi)\,d\xi}{a^2+\xi^2} - a\left[\sqrt{x(\ell-x)} + \ell \tan^{-1}\sqrt{\frac{x}{\ell-x}}\right]\int_o^1 \frac{p(\xi)\,d\xi}{a^2+\xi^2}\right.$$

$$+ 2a\ell \tan^{-1}\sqrt{\frac{x}{\ell-x}}\int_o^1 \frac{\xi^2 p(\xi)\,d\xi}{(a^2+\xi^2)^2} + a^2\ell\left[\ell n\left(\frac{\ell}{\ell-x}\right)\right]\int_o^1 \frac{\xi p(\xi)\,d\xi}{(a^2+\xi^2)^2}$$

$$\left. - 2a^2\ell\int_o^1 \frac{\xi p(\xi)}{(a^2+\xi^2)^2}\,\ell n\left|1 - \frac{a}{\xi}\sqrt{\frac{x}{\ell-x}}\right| d\xi\right\}.$$

For the second foil E = 0 and p(t) = m p(t) in this formula. When K = 0,

$$\eta(x) = \alpha x - y_c(1)\sqrt{x} - \frac{1}{\pi}\left\{\sqrt{x}\int_o^1 p(\xi)\,d\xi + \int_o^1 \xi p(\xi)\,\ell n\left|1 - \frac{\sqrt{x}}{\xi}\right| d\xi\right\}$$

for the first foil. For the second foil $y_c(1) = 0$ and $C_o = \alpha - \frac{2(1-m)C_L}{\pi}$ from Eq. (19). Hence we find

$$\eta(x) = C_o x - \frac{m}{\pi}\left\{\sqrt{x}\int_o^1 p(\xi)d\xi + \int_o^1 \xi p(\xi)\,\ell n\left|1 - \frac{\sqrt{x}}{\xi}\right| d\xi\right\}.$$

Similar formulas for the upper surface of the cavity are obtained from Eq. (23):

$$y(x) = -\left(\frac{B}{2} + D\right) x + aB\left[\sqrt{x(\ell-x)} - \ell \tan^{-1}\sqrt{\frac{x}{\ell-x}}\right] + E\sqrt{x(\ell-x)}$$

$$+ \frac{1}{2\pi(1+K)}\left\{x\int_0^1 \frac{tp(t)dt}{t^2+a^2} + a\left[\sqrt{x(\ell-x)} + \ell \tan^{-1}\sqrt{\frac{x}{\ell-x}}\right]\int_0^1 \frac{p(t)dt}{t^2+a^2}\right.$$

$$- 2a\ell \tan^{-1}\sqrt{\frac{x}{\ell-x}}\int_0^1 \frac{t^2p(t)dt}{(t^2+a^2)^2} + a^2\ell\left[\ell n \frac{\ell}{\ell-x}\right]\int_0^1 \frac{tp(t)dt}{(t^2+a^2)^2}$$

$$\left. - 2a^2\ell \int_0^1 \frac{tp(t)}{(t^2+a^2)^2}\, \ell n\left(1 + \frac{a}{t}\sqrt{\frac{x}{\ell-x}}\right) dt\right\};$$

For the second foil we put E = 0, p(t) = m p(t) and add the term $-2a^2\ell$ A F_1 as indicated in Eq. (23). When K = 0, we find for the first foil that

$$y(x) = y_c(1)\sqrt{x} + \frac{1}{\pi}\left\{\sqrt{x}\int_0^1 p(t)dt - \int_0^1 tp(t)\, \ell n\left(1 + \frac{\sqrt{x}}{t}\right) dt\right\}.$$

In the case of the second foil we put $y_c(1) = 0$, p(t) = m p(t) and add $\frac{1-m}{\pi} C_L \left\{(1-2x)\, x^{\frac{1}{4}}\sqrt{1+\sqrt{x}} - 2x - \ell n\left(x^{\frac{1}{4}} + \sqrt{1+\sqrt{x}}\right)\right\}$ on the left hand side of this equation. These cavity ordinates are measured with respect to the x-axis. In order to obtain offsets from the profile chord-line we may form the sum,

$$y(x) + x\alpha .$$

Appendix C

UPPER CAVITY CONTOUR FOR OFF-DESIGN CONDITIONS

At off-design flow conditions the coefficient A of Eq. (1) is not generally zero. The camber function $\eta(x)$ is now regarded as determined by the preceding inverse calculations so that we can compute the derivative

$$\frac{d\eta}{dx} = V(x)$$

once and for all. The shape of the upper free streamline may be determined from the solution of the direct problem[7] corresponding to the profile slope $V(x)$. For our purposes it seems best to use an integral representation for this solution rather than the series form of Eq. (1). The six fundamental conditions listed previously must still be satisfied by this direct solution. In particular, condition (iv) for closure leads to the relationship,

$$\alpha = a\beta + \frac{1}{2\pi}\left[-\frac{a}{2}\delta + \frac{2a^2}{\delta} + \frac{a\epsilon}{\delta^2}\right] I_1 + \frac{1}{2\pi}\left[-\frac{\delta}{2} + \frac{2a}{\delta} + \frac{\epsilon}{\delta^2}\right] I_2$$

$$+ \frac{2}{\pi}\frac{1}{\delta} I_3 + \frac{2}{\pi}\frac{\epsilon}{\delta^2} I_4 , \qquad \text{(C1)}$$

where, as before,

$$\begin{Bmatrix} \delta \\ \epsilon \end{Bmatrix} = \left[\sqrt{\ell}+1\right]^{1/2} \pm \left[\sqrt{\ell}-1\right]^{1/2} .$$

The integrals I_1 through I_4 are defined by

$$I_1 = \int_0^1 \frac{V(x)\,dx}{x^{1/4}\left[\sqrt{\ell-x} - a\sqrt{x}\right]^{1/2}\sqrt{\ell-x}} ,$$

$$I_2 = \int_0^1 \frac{x^{1/4}\, V(x)dx}{[\sqrt{\ell-x} - a\sqrt{x}]^{1/2}\,(\ell-x)} ,$$

$$I_3 = \int_0^1 \frac{\sqrt{\ell-x}\, V(x)dx}{x^{1/4}\,[\sqrt{\ell-x} - a\sqrt{x}]^{1/2}} ,$$

and

$$I_4 = \int_0^1 \frac{x^{1/4} V(x)dx}{[\sqrt{\ell-x} - a\sqrt{x}]^{1/2}} .$$

For values of $\underline{a}$, α and β satisfying Eq. (C1) the value of the coefficient A is given by

$$A = -\frac{1}{2}\sqrt{\frac{a}{a^2+1}}\left[\alpha\delta + \beta\epsilon + \frac{\sqrt{\ell}}{\pi} I_2\right] ,$$

and for B we must replace Eq. (18) by the formula,

$$B = \frac{\delta - a\epsilon}{2a\sqrt{\ell a}}\alpha - \frac{1}{4\pi a\sqrt{\ell a}}\left[\frac{\delta-a\epsilon}{2}\epsilon - (2a^2+1+\frac{a\epsilon}{\delta})\right] I_1$$

$$+ \frac{1}{4\pi a\sqrt{\ell a}}\left[\frac{\delta-a\epsilon}{2}\delta - (\frac{\epsilon}{\delta}+a)\right] I_2 - \frac{1}{\pi a\sqrt{\ell a}} I_3 - \frac{1}{\pi a\sqrt{\ell a}}(\frac{\epsilon}{\delta}) I_4 .$$

After an integration the ordinates of the upper surface of the cavity measured from the profile chord are given by

$$y(x) = -2a^2\ell\left\{AF_1(\nu,a) + BF_2(\nu,a)\right\} - J_1I_1 - J_2I_2 - J_3I_3 - J_4I_4$$

$$+ \frac{1}{\pi}\int_0^1 V(t)\cos^{-1}\left[\frac{a\sqrt{t} - (\sqrt{\ell-t} - 2a\sqrt{t})\nu}{a\sqrt{t} + \nu\sqrt{\ell-t}}\right] dt , \qquad (C2)$$

where $\nu(x)$ is determined by Eq. (2) with $z = x \geq 0$. The functions F_1 and F_2 are defined by*

$$F_1(\nu,a) = \frac{1}{2a^2}\left[\frac{\nu\sqrt{\nu(\nu+1)}}{\nu^2+a^2} + \frac{\beta_1}{4\omega^2}L(\nu,a) + \frac{\beta_2}{2\omega^2}T(\nu,a)\right],$$

and

$$F_2(\nu,a) = -\frac{\sqrt{\nu(\nu+1)}}{2(\nu^2+a^2)} + \frac{1}{4\omega^2}\left(\beta_1 - \frac{\beta_2}{2a}\right)L(\nu,a) + \frac{1}{4\omega^2}\left(2\beta_2 + \frac{\beta_1}{a}\right)T(\nu,a),$$

where

$$\omega^2 = a\sqrt{\ell},\ \beta_1 = -\sqrt{\frac{\omega^2-a^2}{2}},\ \beta_2 = -\sqrt{\frac{\omega^2+a^2}{2}},\ \delta_1 = \frac{a\beta_2}{2\omega^2}$$

$$\delta_2 = \frac{a\beta_1}{2\omega^2},\ \gamma_1 = \frac{1}{\omega^2}\left(a\beta_2+\frac{1}{2}\beta_1\right) \text{ and } \gamma_2 = \frac{1}{\omega^2}\left(a\beta_1 - \frac{1}{2}\beta_2\right).$$

The functions L and T are given by

$$L(\nu,a) = \ell n\left\{a^2\left[\frac{(\gamma_1\nu + \delta_1 - \sqrt{\nu(\nu+1)})^2 + (\gamma_2\nu+\delta_2)^2}{(\delta_1^2+\delta_2^2)(\nu^2+a^2)}\right]\right\}$$

and

$$T(\nu,a) = \tan^{-1}\frac{\gamma_2\nu+\delta_2}{\gamma_1\nu+\delta_1-\sqrt{\nu(\nu+1)}} = \tan^{-1}\frac{\delta_2}{\delta_1} - \tan^{-1}\frac{\nu}{a}.$$

*The function $T(\nu,a)$ is not to be confused with the trailing edge thickness, T, of Eq. (27).

The J functions are:

$$J_1 = -\frac{\ell a^{3/2}}{\pi} F_2(\nu,a), \quad J_2 = \frac{\ell a^{5/2}}{\pi} F_1(\nu,a)$$

$$J_3 = \frac{a^{3/2}}{\pi}\left\{\frac{1}{2\omega^2}\left(\beta_1 - \frac{\beta_2}{a}\right) L(\nu,a) + \frac{1}{\omega^2}\left(\beta_2 + \frac{\beta_1}{a}\right) T(\nu,a)\right\}$$

and

$$J_4 = \frac{a^{1/2}}{\pi}\left\{\frac{\beta_1 + a\beta_2}{2\omega^2} L(\nu,a) + \frac{\beta_2 - a\beta_1}{\omega^2} T(\nu,a)\right\} .$$

In the case of K = 0, for which $\underline{a} = \infty$, the formulas are greatly simplified. Thus, when K = 0, y_u is given by

$$y_u(x) = \frac{\alpha}{2}\left\{(2\sqrt{x}+1)\, x^{1/4}\sqrt{1+\sqrt{x}} - \ell n\left|x^{1/4}+\sqrt{1+\sqrt{x}}\right|\right\}$$

$$-\frac{1}{\pi}\left\{x^{1/4}\sqrt{1+\sqrt{x}} + \ell n\left|x^{1/4}+\sqrt{1+\sqrt{x}}\right|\right)\int_0^1 \frac{V(t)\,dt}{t^{1/4}\sqrt{1-\sqrt{t}}}$$

(C3)

$$-2\ell n\left|x^{1/4}+\sqrt{1+\sqrt{x}}\right| \int_0^1 \frac{t^{1/4}V(t)\,dt}{\sqrt{1-\sqrt{t}}} + \int_0^1 V(t)\cos^{-1}\left(\frac{(1+2\sqrt{x})\sqrt{t}-\sqrt{x}}{\sqrt{x}+\sqrt{t}}\right)dt\Big\} ,$$

where again the cavity ordinates are measured with respect to the chord line.

The preceding formulas can be used to distinguish those flow states (i.e., those values of α, K and $\underline{a}$) which lead to interference between the cavity and the upper surface of the profile from those which do not. For example when K > 0, we have Eq. (C1) which is of the form,

$$\alpha = a\beta + W(a), \qquad (C5)$$

where W is a function of $\underline{a}$ only. Equation (C5) must always be satisfied in the direct problem of closed cavity theory if α, β and $\underline{a}$ are to have admissible values. On the other hand, the upper surface of the cavity follows from (C2) and can be put in the form

$$y_{\blacksquare}(x) = \underset{\sim}{\tilde{I}}_1 \beta - \underset{\sim}{\tilde{I}}_2 , \tag{C6}$$

where $\underset{\sim}{\tilde{I}}_1$ and $\underset{\sim}{\tilde{I}}_2$ are functions of x and $\underline{a}$. Let us require that in the interval, $0 \leq x \leq 1$, there is one value of x for which

$$y_{\blacksquare}(x) = t(x) . \tag{C7}$$

The function t(x) defines the upper surface of the foil with respect to the chord line. A convenient choice for this function is

$$t(x) = \theta y(x)\big|_d ,$$

where $y(x)\big|_d$ is the upper surface of the cavity at the design point in accordance with either the first or the second design method and where θ is a positive number less than or equal to unity. Equation (C6) implies that the cavity is tangent to the upper surface of the foil at one or possibly more points and that the cavity does not cut the upper surface of the foil. Therefore, at some values of x we have from (C6) that

$$\beta_{\blacksquare\blacksquare} = \frac{t(x) + \underset{\sim}{\tilde{I}}_2 (x,a)}{\underset{\sim}{\tilde{I}}_1 (x,a)} ,$$

If we choose a value of $\underline{a}$, we can calculate a value of β for each x in (o, x). We can select the largest value of β from among these values. Then using the same $\underline{a}$ value we can use this value of β in Eq. (C5) to calculate a value of α. These three values ($\underline{a}$, β and α) define a flow state at which the cavity is just tangent to the hydrofoil. This calculation can be repeated for a sequence of $\underline{a}$-values to

define a locus of points which divides an α-K plane into two regions, corresponding to permissible flow states and those leading to interference between the foil and the cavity. The actual equations and methods of calculation are discussed in Ref. 5.

REFERENCES

1. Tulin, M. P. and M. P. Burkart, Linearized Theory for Flows About Lifting Foils at Zero Cavitation Number, David Taylor Model Basin Report No. C-638, Feb. 1955.

2. Johnson, V. E., Jr., "The Influence of Depth of Submersion, Aspect Ratio, and Thickness on Supercavitating Hydrofoils Operating at Zero Cavitation Number," Proc. Second Symposium on Naval Hydrodynamics, ACR-38, Office of Naval Research, Department of the Navy, Washington, D. C., 1958, p. 317.

3. Auslaender, J., "The linearized Theory for Supercavitating Hydrofoils Operating at High Speeds Near a Free Surface," Jnl. of Ship Research, Vol. 6, No. 2, Oct. 1962, p.8.

4. Oba, R., "Theory for Supercavitating Flow Through an Arbitrary Form Hydrofoil," read at the Aviation and Space, Hydraulic and Gas Turbine Conference, ASME, Los Angeles, Calif., March 1963.

5. Grote, R. S., Numerical Methods and Program Description for the Inverse Problem of Linearized, Fully-Cavitating, Hydrofoil Theory, The RAND Corporation, RM-3563, September 1964.

6. Fabula, A. G., Application of Thin-airfoil Theory to Hydrofoils with Cut-off Ventilated Trailing Edge, NOTS T.P. 2547, NAVWEPS Report 7571, U. S. Naval Ordnance Test Station, China Lake, California, Sept., 13, 1960.

7. Parkin, B. R., "Munk Integrals for Fully Cavitated Hydrofoils," Jnl. of the Aerospace Sciences, Vol. 29, No. 7, July 1962, p. 775.